Topographical Analysis of the Frontal Terminations of the Language Network: Insights on Anatomical and Methodological Variability

Eva Guzmán Chacón
Supervisor: Dr. Stephanie J. Forkel
Second Reader: Dr. Vitória Piai

Radboud University, The Netherlands

August 2024

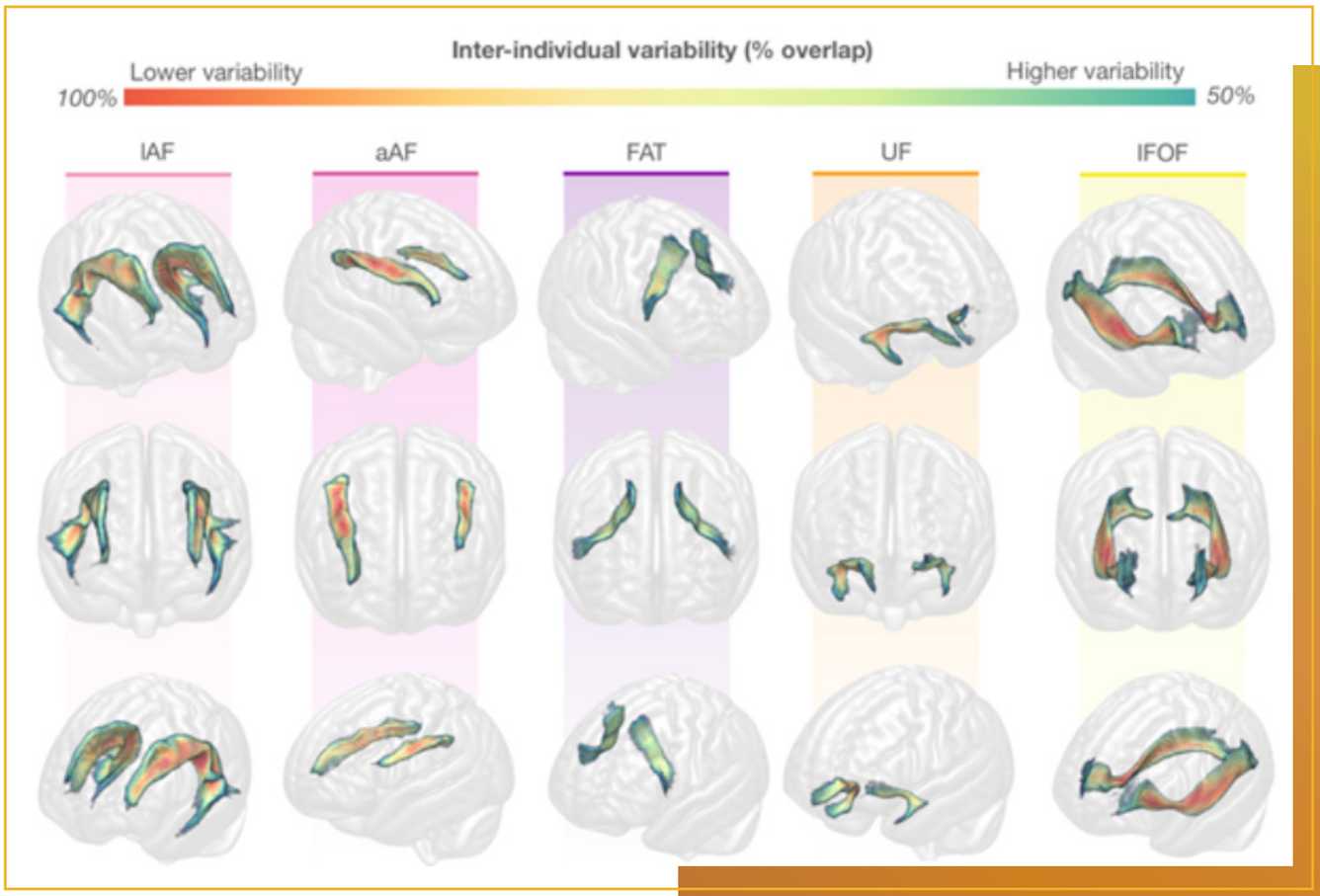
Inter-individual variability (% overlap)
Lower variability
Higher variability
100%
50%
IAF
aAF
FAT
UF
IFOF

Abstract

Despite over a century of research, the precise anatomy of language in the human brain remains partially understood. The gap persists due to the lack of large datasets with a focus on language mapping and the need for novel tools that can more precisely capture connectional anatomy. This study leverages the Language in Interaction dataset and advanced tractography using high-angular resolution imaging (HARDI) to examine the anatomical properties and frontal terminations of the extended language network in 198 healthy participants. Our analysis focused on mapping the patterns of variability and laterality of five bilateral frontal lobe tracts associated with language: the long and anterior segments of the arcuate fasciculus (AF), the frontal aslant tract (FAT), the inferior fronto-occipital fasciculus (IFOF), and the uncinate fasciculus (UF). We employed two tractography algorithms —spherical deconvolution (SD) and diffusion tensor imaging (DTI)—, alongside manual and semi-automated (MegaTrack) dissection techniques, to estimate interindividual and methodological variability of the dissections. The frontal lobe was almost entirely within the cortical reach area of the language network, and its tracts displayed significant asymmetries and complex termination patterns that challenge classical models. The use of ICA provides a nuanced framework for understanding these anatomical variations, pointing to an intricate integration of the language network with other cognitive functions. These results can crucially inform neurolinguistic theories and potentially aid interventions for language-related disorders long-term.

Keywords: Language Network, Frontal Terminations, Tractography, White Matter, Variability

Abbreviations:

aAF - Anterior segment of the arcuate fasciculus
AP - Power of anisotropy
DTI - Diffusion tensor imaging
DWI - Diffusion weighted imaging
FA - Fractional anisotropy
FAT - Frontal aslant tract
HMOA - Hindrance-modulated orientational anisotropy
IFOF - Inferior fronto-occipital fasciculus
lAF - Long segment of the arcuate fasciculus
MRI - Magnetic Resonance Imaging
SD - Spherical deconvolution
T1w - T1 weighted
UF - Uncinate fasciculus

1 Introduction

Language anatomy, encompassing the neural structures and pathways involved in language processing, is crucial for the improvement of neurolinguistic models and clinical outcomes. Previous studies have highlighted the significance of anatomical interindividual variability and laterality of white matter pathways in determining clinical outcomes, particularly in the context of language recovery after brain injury (S. J. Forkel, Thiebaut de Schotten, Dell'Acqua, et al., 2014; Talozzi et al., 2023). Understanding each tract's cortical area of connectivity (terminations) can be crucial in surgical scenarios and is worth mapping through various techniques, as emphasised by Giampiccolo Duffau (2022). Their work inspired our examination of the controversial frontal terminations of the language network through spherical deconvolution tractography (de Benedictis et al., 2021; Dell'Acqua et al., 2013; Giampiccolo and Duffau, 2022; Shekari and Nozari, 2023). Given the role of the frontal lobe in higher-order cognitive functions, including decision-making, learning, and creativity (Collins and Koechlin, 2012), exploring frontal connectivity within the language network has the potential to provide valuable insights into the 'language ready brain' (Hagoort, 2013), offering a unique perspective on the broader cognitive processes that shape human communication.

1.1 Extending the language network

Regions such as the so-called Broca's area (inferior frontal gyrus, BA 44/45), Wernicke's area (superior temporal gyrus, BA 21/22), and their connections through the arcuate fasciculus have long governed the neuroanatomical understanding of language (Dick and Tremblay, 2012). However, more recent works have advocated for a more holistic model of language, extending beyond the classical cortical areas and expanding beyond the AF (Catani et al., 2005; Dick and Tremblay, 2012; S. J. Forkel and Catani, 2019; Hagoort, 2019; Shekari and Nozari, 2023). This shift was greatly influenced by lesion or intraoperative observation in pathological populations. However, clinical observations are at odds with current models of the neurobiology of language in the healthy population. Thanks to the advent of novel neuroimaging methods that allow the study of the connectional anatomy of the brain, the study of the subcortical network of language processing has gained momentum.

New models have been proposed (Catani and Bambini, 2014; Duffau et al., 2014; Hickok and Poeppel, 2004; Ueno et al., 2011) coming from the fields of psychiatry (Catani and Bambini, 2014), neurosurgery (Duffau et al., 2014), computational neurology (Ueno et al., 2011), and linguistics (Hickok and Poeppel, 2004). The prevailing model includes a language network comprised of two main processing streams (Figure 1): the dorsal stream for phonological and syntactic processing (sound to action) and the ventral stream for semantic processing (sound to meaning; Hickok and Poeppel, 2004, Hickok and Poeppel, 2007). The anatomical basis of the dorsal stream is considered to include a fronto-temporal tract, the arcuate fasciculus (AF; Catani et al., 2005), and a frontal intra-lobular tract, the frontal aslant tract (FAT; Catani et al., 2012; Oishi et al., 2008). On the other hand, the ventral stream consists of the inferior fronto-occipital fasciculus (IFOF, S. J. Forkel, Thiebaut de Schotten,

Dell'Acqua, et al., 2014), the uncinate fasciculus (UF, Catani and Thiebaut de Schotten, 2008), and the inferior longitudinal fasciculus (ILF,Catani et al., 2003), out of which, only the IFOF and UF have connections (terminations) within the frontal lobe.

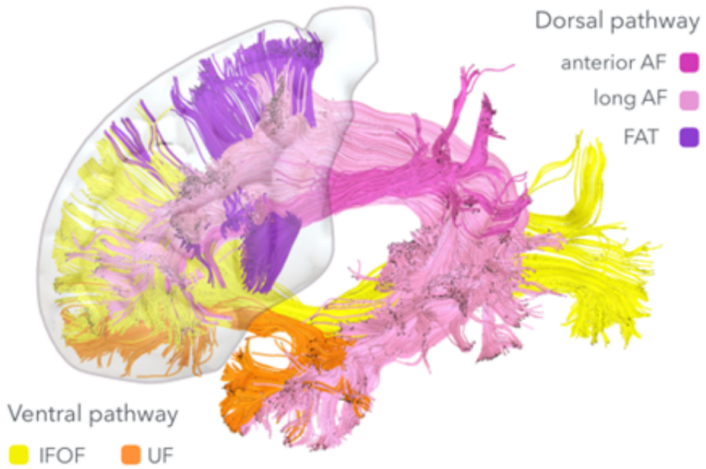

Figure 1: Language Network: Frontal lobe connections

Note: White matter tracts with frontal terminations belonging to the dorsal and ventral pathways of the language network. Exemplary dissections of one participant from the Language in Interaction BQ4 dataset. AF: arcuate fasciculus, FAT: frontal aslant tract, IFOF: fronto-occipital fascicle, UF: uncinate fasciculus.

1.2 Methodological barriers in understanding cortical terminations

Nevertheless, despite our confidence in the supportive role of these tracts in language processing, there is currently a lack of a definitive method for their precise structural characterisation (Giampiccolo and Duffau, 2022). Anatomical descriptions through post-mortem dissections remain heavily dependent on the quality of the specimen, are time-consuming, and require extensive experience (Dell'Acqua and Catani, 2012; Türe et al., 2000). The non-invasive in-vivo alternative, diffusion weighted imaging (DWI), is a magnetic resonance imaging (MRI) technique used for tractography reconstructions. Tractography allows for the study of the brain's white matter tracts and atlasing of its structural connectivity. An advanced technique for tractography, spherical deconvolution (SD), is based on High Angular Resolution Imaging (HARDI) and is able to model multiple fibre orientations within each voxel (Dell'Acqua et al., 2013; Dell'Acqua and Tournier, 2019). Multifibre orientations allow for more accurate tracing of complex fibre pathways in areas of fibre crossing (90% of the brain, Jeurissen et al., 2013). This constitutes an improvement to previous algorithms such as classical diffusion tensor imaging (DTI), which are limited to reconstructing single fibre orientations. Still, DWI offers little information close to the cortex given the sudden increase in diffusivity and the limited resolution of the images (typically acquired with 2mm voxels, which is very similar to the average thickness of the

cortex), leading to difficulties in determining the exact terminations of the. Therefore, the absence of a gold standard, a universally accepted reference or benchmark, makes it difficult to validate and compare findings across different studies (Dell'Acqua and Catani, 2012; Dziedzic et al., 2021; Yendiki et al., 2022). Klingler post mortem dissections were long thought of as the gold standard but suffer similar limitations as tractography (Dell'Acqua and Catani, 2012) while tracing studies are only feasible in other species (Yendiki et al., 2022) and not necessarily useful in the context of language since we expect differences across species that annul the translatability of results.

Given these limitations, many controversies still surround the exact cortical terminations of white matter tracts (de Benedictis et al., 2021). Fortunately, conflicting evidence in the literature is also accompanied by efforts to reach a consensus. For instance, Vavassori et al. (Vavassori et al., 2021) reviewed the historical literature on the superior longitudinal system, and compared the different models with regards to their frontal, temporal, and parietal terminations. They not only identify the changing, conflicting, and overlapping descriptions of the AF and the superior longitudinal fasciculus (SLF), but they also stress the importance of agreeing on a given paradigm in order for research in neurosurgical and clinical fields to advance. More recently and with these implications in mind, Giampiccolo Duffau Giampiccolo and Duffau, 2022 revisited the temporal terminations of the left AF combining various sources of evidence, including anatomical dissections, diffusion tractography, functional MRI and intraoperative mapping studies. This review solidified the case for a far-reaching AF that extends beyond the traditional temporal terminations in Wernicke's area or superior temporal gyrus. Given the reviewed functional correlates, the authors stress the importance of sparing the full extent of the AF for language preservation (Giampiccolo and Duffau, 2022).

A network approach to studying these controversies provides a more well-rounded perspective of the language connectome, as exemplified by Vassal et al. (Vassal et al., 2026) who used DTI tractography of 20 healthy volunteers to describe frequent occurrences of connection patterns for eight white matter fascicles of the language network. They thoroughly report the occurrence of connections to a set of parcellated areas for each fascicle and identify prominent hemispheric asymmetries. For instance, AF comprised direct connections between Broca's (BA 44/45) and Wernicke's (BA 21/22) areas in all left hemispheres but only 40% of right hemispheres. Although these observations were insightful at the network-level, their sample size could not answer the question of how the cortical projections of the language connectome might differ from one healthy brain to another, which could lead to advances in phenotyping white matter and impact our understanding of clinical cases (S. J. Forkel, Thiebaut de Schotten, Kawadler, et al., 2014).

1.3 Exploring interindividual and methodological variability of cortical terminations

While it has been known to anatomists for a long time that each brain is different, neuroimaging methods were not able to capture this interindividual variability until recently. To investigate this,

Croxson and colleagues (Croxson et al., 2018) mapped a healthy population and demonstrated that variability is not homogenous across the brain and the white matter. Their whole brain analysis identified a gradient of variability with areas of high variability being identified as higher cognitive function areas by neuroimaging and lesion studies (Croxson et al., 2018). This study was however limited to a whole brain analysis and did not identify system-specific patterns of variability, nor did it focus on cortical terminations.

As previously mentioned, the sudden increase in diffusivity and the limited resolution of the images hinders the description of exact streamline termination and their variability. However, white matter streamlines can be extended to the closest surface point to map the corresponding cortical terminations (Beyh et al., 2022). This allows us to jump the interface between grey and white matter, and topographically analyse the distributions of these connections to estimate interindividual variability. It is important to note that current in-vivo tractography still suffers from "gyral bias", whereby fibre tracking algorithms terminate preferentially on gyral crowns, rather than the banks and fundi of sulci (Schilling et al., 2018).

Interindividual variability can be quantified as a whole or further dissected by means of principal and independent component analyses (Beckmann, 2012;Cattell, 1966;Jolliffe and Cadima, 2016). The former is designed to capture patterns in the data that explain the largest amount of variability, whilst the latter primes statistical independence. Here, we applied such methods to terminations in order to establish topographical patterns of connectivity that explain an individual's unique terminations.

In addition to interindividual variability, methodological variability inevitably emerges, stemming from the choice of diffusion algorithm that may produce different outcomes owing to differences in data acquisition, preprocessing, and modelling methodologies. These discrepancies have the potential to influence the precision and dependability of the resulting fibre pathways and connectivity mappings (Tallus et al., 2023). Moreover, the human element could impact the manual virtual dissections due to a person's pre-existing biases, such as what the laterality or extent of specific tracts should be, resulting in variations in the dissections' cleaning process. Consequently, discrepancies may arise in the identification and characterisation of anatomical white matter, posing challenges in fully grasping its organisation and functionality. Efforts to conduct faster group-level dissections led to the development of the semi-automatic MegaTrack software (Dell'Acqua et al., 2015). MegaTrack merges tractograms from several individuals so that a given tract can be simultaneously dissected for all of them and subsequently separated back into individual tracts. This, in turn, can be used to merge tractograms from different reconstruction methods and hemispheres to perform a single dissection free of the aforementioned biases.

In this study, we focused on building a probabilistic model of the frontal terminations of the language network —anatomically determined by diffusion imaging of 198 participants. Our primary focus lies in mapping the interindividual and methodological variability of these tracts and their terminations, carrying out various analyses on microstructural and spatial dimensions. To achieve this,

we employ two imaging reconstruction modalities, DTI and SD, coupled with two dissection techniques (manual and MegaTrack, megatrackatlas.org; Dell'Acqua et al., 2015). The resultant tracts serve dual purposes: being the first external and large-scale validation of MegaTrack against manual dissections and allowing for an analysis of terminations and laterality unaffected by biases. Overall, this study sheds light on the interindividual and methodological variability that shapes our understanding of the frontal terminations of the language white matter network. Such insights hold significant ramifications for contemporary functional models of language and clinical practice.

2 Methods

2.1 Data Acquisition

We used the neuroimaging data from the Language In Interaction BQ4 dataset (n=198, age range 18-30, age average=23, 73% female, languageininteraction.nl). Data were acquired on a 3T Magnetom Prisma MR scanner at the Donders Institute Nijmegen. Structural T1-weighted images were acquired at $1 \times 1 \times 1\ mm^3$ isotropic resolution with a repetition time of 2000 $msec$, an echo time of 2.03 $msec$, a flip angle of 8°, and a field of view of $256 \times 256 \times 192\ mm^3$. Diffusion weighted imaging (DWI) data were acquired using a spin-echo echo planar imaging sequence with an echo time of 74.8 $msec$, repetition time of 2940 $msec$, a field of view of $216 \times 216\, mm^2$, 81 slices, isotropic voxels of $1.8 \times 1.8 \times 1.8\ mm^3$, in-plane acceleration factor 2, multi-band factor 3, 86 gradient directions at b = 1250 $s{\cdot}mm^{-}2$, 85 directions at b = 2500 s·mm-2, 11 b = 0 images, and 7 b = 0 images with reversed phase encoding.

2.2 Diffusion Weighted Image Preprocessing and Processing

The raw DWI data were corrected for thermal noise (Veraart et al., 2016) and Gibbs ringing artefacts (Kellner et al., 2016). b0 images with reverse phase encoding polarity were used to estimate the susceptibility distortion field using topup (Andersson et al., 2003). eddy was used to correct the DWI series for eddy current distortions, motion artefacts, slice-to-volume motion, outlier slice regeneration, and incorporating the topup field into this step, including the effects of motion on these distortions (Andersson et al., 2016;Andersson and Sotiropoulos, 2016; Andersson et al., 2017; Andersson et al., 2018).

Anisotropic power (AP) maps (Dell'Acqua et al., 2014) derived from the pre-processed DWI images were used to estimate a rigid body alignment between the DWI space and the T1w space in ANTs (Avants et al., 2011; Avants et al., 2014). The resulting transformation was applied to the entire DWI series using spline interpolation. The b-vectors were also rotated according to the same transformation.

Damped Richardson-Lucy spherical deconvolution modelling (Dell'acqua et al., 2010) and deterministic tractography were performed using StarTrack (mr-startrack.com) and the following parameters:

fibre response α = 1.5; number of iterations = 200; minimum amplitude threshold η = 0.0015; regularisation threshold ν = 16; step size = 1 mm; absolute threshold for tracking = 0.002; maximum angle threshold = 45°; minimum length = 20 mm; maximum length = 300 mm. Within the same software, diffusion tensor modelling and tractography were applied with the following parameters: step size = 0.9 mm; minimum FA threshold = 0.15; angle threshold = 35°; minimum length = 20 mm; maximum length = 300 mm.

AP maps computed during modelling were used to calculate a diffeomorphic registration between native space anatomy and the MNI152 T1w template. This step was performed in ANTs using the SyN algorithm (Avants et al., 2011). The resulting transformations were applied to the whole brain tractogram using in-house MATLAB scripts. This yielded the final tractograms that were used for manual virtual dissections in TrackVis (trackvis.org).

To prepare for the MegaTrack analysis, an additional registration step was performed to map each tractogram to the ICBM 2020 Nonlinear symmetric brain template (Fonov et al., 2011) where the left and right hemispheres are mirror images of each other. This was achieved by mapping the MNI152 template to this symmetric template using ANTs. Thereafter, any tractogram could be registered to the symmetric template via a two-step registration: native → MNI152 (asym.) → ICBM (sym.).

2.3 Data Analysis

2.3.1 Manual Dissections

The final tractograms were visualised in Trackvis (trackvis.org) and manually dissected according to previous literature (Catani and Thiebaut de Schotten, 2008; S. Forkel et al., 2024; Rojkova et al., 2016). Over a period of four months, we dissected the prominent language tracts connected to the frontal lobe, resulting in five tracts in each hemisphere: long and anterior segments of the arcuate fasciculus, inferior fronto-occipital fasciculus, uncinate fasciculus, and frontal aslant tract. The regions of interest (ROIs) used for dissection were predefined in MNI space under the supervision of an expert anatomist (SJF) (Figure 2). Briefly, the long segment of the AF was defined as a fronto-temporal pathway, with two-dimensional ROIs in the precentral gyrus and at the posterior section of the temporal lobe. Similarly, the IFOF was dissected with a ROI on the occipital lobe and another in the external/extreme capsule. The latter ROI is also used in combination with a sphere in the temporal pole for the delineation of the UF. Two more spheres were placed on the inferior precentral gyrus and Geshwind's territory in the inferior parietal lobe to dissect the anterior segment of the AF. Lastly, the FAT was dissected with ROIs spanning the posterior inferior frontal gyrus and the superior frontal gyrus. Crucially, all 10 dissected tracts of each participant were individually examined and cleaned of artefacts with additional "NOT" ROIs.

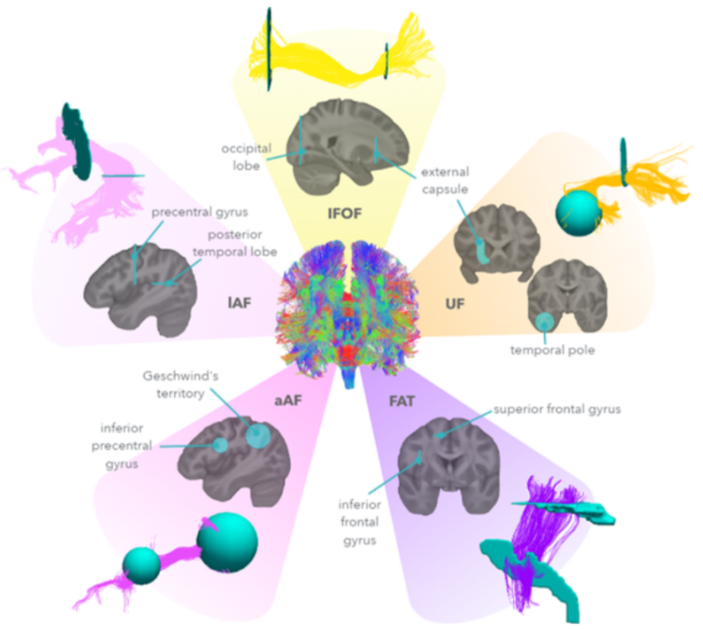

Figure 2: Regions of interest used for manual segmentation

Note: Each full tractogram is segmented into 5 bilateral tracts with the use of two inclusive regions of interest per tract. The regions were determined in MNI space. aAF: anterior segment of the arcuate fasciculus, lAF: long segment of the arcuate fasciculus, FAT: frontal aslant tract, IFOF: fronto-occipital fascicle, UF: uncinate fasciculus.

In order to analyse the extent of cleaning required in each tract, dissections and their visitation maps (i.e. a map showing each voxel intersected by a streamline) were saved before and after this process to compute the difference in streamline count and volume, as well as to spatially describe the areas consistently discarded.

Following previously described analyses (Thiebaut de Schotten et al., 2011), we assessed group effects by computing statistical maps for each white matter tract. Briefly, dissected tracts were transformed into binary visitation maps in which each voxel is assigned a value of 1 or 0 based on the presence or absence of a streamline in that specific location. Subsequently, a permutation-based one-sample t-test was conducted on these maps utilising FSL's randomise tool with 5000 permutations (Winkler et al., 2014). This approach facilitated the derivation of statistically significant maps and effect size maps (Cohen's d), which were then restricted to the areas of significant effect ($p < 0.05$ voxel-wise corrected for family-wise error).

Additionally, we summed all binary visitation maps into percentage overlap maps, filtered at a 50% threshold, where variability reflected interindividual overlap variability (Thiebaut de Schotten et al., 2011).

From this data, we extracted tract-specific measurements which included median fractional anisotropy (FA), number of streamlines, volume, anisotropy power (AP) and Hindrance Modulated Orienta-

tional Anisotropy (HMOA) for the complete tract (Dell'Acqua et al., 2013). We calculated a lateralisation index for each metric according to the following formula:

$$(metric_R - metric_L)/(metric_R + metric_L)$$

In line with the pipeline by Thiebaut de Schotten et al. (Thiebaut de Schotten et al., 2011), we assessed the statistical significance of the degree of the lateralisation of each tract and metric using one-sample t-tests. Additionally, we performed an analysis of variance analysis (ANOVA) to test the sex differences in the lateralisation indexes independently for each tract and metric. Finally, Bonferroni correction was applied to account for multiple comparisons.

2.3.2 Cortical Projections of the Language Network

Cortical projections were computed as described in Beyh et al. (Beyh et al., 2022). Native space Freesurfer cortical meshes were re-tessellated to match the '32k FS LR' surface template using tools from Connectome Workbench (humanconnectome.org/software). The '32k FS LR' template is a standardised cortical surface model that features $\sim$ 32k vertices per hemisphere and maintains the native anatomical features of each brain while facilitating precise vertex-level correspondence and comparison between participants. Next, the end points of each streamline were projected to their nearest neighbour surface vertex within a radius of $2.5\,mm$. These projection maps were then smoothed along the surface with a geodesic Gaussian kernel (FWHM = $2mm$) in order to compensate for the sparsity with which streamlines reach the cortical surface and to account for the uncertainty of the projection location (Jones, 2003).

These projection maps were binarised and masked for the frontal lobe in order to be used as input for subsequent component analyses as well as the computation of a frontal termination area laterality index following the previously mentioned formula. Such indexes were used along streamline count and volume laterality indexes to form a linear model and explore the intercept and residuals. A final surface-wise smoothing (FWHM = $4\,mm$) was applied to the maps for the calculation of the surface Cohen's d maps.

2.3.3 Termination Component Analysis

In order to identify anatomical patterns in the tracts and terminations that are not apparent to the naked eye, dimensionality reduction methods were applied. In particular, independent component analysis (ICA; Beckmann, 2012) is a linear method that primes the statistical independence of components. This method is most efficient when performed on whitened data —where correlations are removed and variance always equals one— since some operations such as scaling will not be necessary during the ICA. After whitening, ICA only needs to perform a rotation of the data matrix and will converge faster. Whitening can be achieved by applying a principal component analysis (PCA;

Jolliffe and Cadima, 2016) that focuses on explaining the most variance through orthogonal components. Hence, a PCA analysis was performed on the vertices belonging to the frontal lobe for each of the 5 tracts and hemispheres. Then, the first 50 components of terminations were used as whitened input for the ICA analysis rendering 5 termination components per tract.

UMAP (Uniform Manifold Approximation and Projection) is an advanced dimensionality reduction tool that non-linearly generates an embedding space that retains the original distances in the data (McInnes et al., 2020). To see if this method could use prior analyses to phenotype participants in terms of their terminations, we constructed an embedding space with 2 and 3 components based on the final set of 50 language network independent component scores.

2.3.4 Behavioural Factor Scores

To probe the association between micro and macrostructural metrics and indexes in the white matter of the healthy brain, we used factor scores derived from each individual's raw behavioural scores from the Language in Interaction dataset (Hintz et al., 2020). These factor scores include Word Production, Sentence Comprehension, Linguistic Knowledge, Processing Speed, Working Memory, Corsi Digit Span, and IQ. A linear mixed-effects model was used to find relationships between such scores (dependent variable) and laterality indexes of HMOA, FA, streamline count, and volume, as well as the individual hemispheric metrics (independent variables), while accounting for the random effects of interindividual variability. Finally, factor scores were correlated against the ICA components.

2.3.5 MegaTrack

Manual dissections have the advantage of being more individualised and informed by prior anatomical knowledge of the tracts and tractography reconstruction characteristics. On the other hand, there might be a question of a slight bias when dissecting DTI vs. SD (i.e. by being more lenient on SD dissection cleaning) or left vs. right hemisphere (i.e. previous knowledge of laterality accentuating the results). In order to explore this effect and perform dissections of both DTI and SD data and of both hemispheres without implicit laterality or reconstruction-type bias, we used the MegaTrack tool (megatrackatlas.org; Dell'Acqua et al., 2015). MegaTrack combines tractography data from multiple participants into a single, standardised anatomical space, resulting in a "mega" tractogram and enabling simultaneous dissection of the whole dataset. Each streamline in the MegaTrack dataset is tagged with unique identifiers, allowing for the recovery of native space tracts and the automatic extraction of tract-specific measurements. In this case, we built a dataset using a symmetric brain template so both modalities (DTI and SD) and hemispheres could be combined into a single dense tractogram to be dissected at once, without knowledge of what streamlines belong to each hemisphere or reconstruction type. The ROIs used were akin to those used on the manual segmentations, allowing for a direct comparison of the results.

As the first external validation of the MegaTrack software, we computed the weighted Dice coefficient of similarity between MegaTrack's output and manual dissections, which is considered the gold standard in this context. The weighted version of Dice, as described in Cousineau et al. (Cousineau et al., 2017), gives more importance to voxels, indicating a high density of streamlines, that is, the core of the tracts, rendering more reliable results. Additionally, micro and macrostructural metrics were correlated for each tract to establish if the distribution of the data is maintained across dissection methods.

We then used the generated dissections to explore the possibility of a laterality bias inflicted by the person dissecting during manual cleaning. Laterality bias was conceptualised as the intercept of a linear model containing the unbiased laterality (from MegaTrack) as a predictor and the laterality obtained from the manual dissections as the outcome.

Lastly, we compare DTI and SD dissections performed simultaneously in MegaTrack in terms of laterality metrics, spatial similarity (weighted Dice coefficient), and cortical termination areas (Cohen's d).

3 Results

3.1 Manual Dissections

All tracts were successfully dissected for each of the 198 participants. In the case of the UF, some instances rendered very few streamlines, but these cases were kept in the dataset as a representation of typical interindividual or tractographic variability.

It is common in tractography reconstructions for tracts to merge with each other, generating anatomically incorrect streamlines. Additionally, due to the densely packed nature of white matter, ROI selection is not flawless and can sometimes lead to encompassing undesired streamlines. Therefore, a substantial cleaning effort was carried out using "NOT" ROIs to ensure the anatomical plausibility of the dissections (Figure 3A). The extent of such cleaning is sometimes as high as 50% (left UF), and the volume metric is more susceptible to this process since most of the cleaned fibres stray from the main body of the tract (Figure 3B). Moreover, this figure emphasises that the need for pruning in the left hemisphere was consistently higher than in the right. Out of the 5 tracts, the FAT turned out to render the cleanest raw dissection, requiring close to no cleaning and lacking reproducible artefacts. For the rest of the tracts, on the other hand, Figure 3C shows the voxels that were discarded in at least 10% of the individuals. Insular connections were frequently found in the raw AF dissections, and the raw IFOF and UF frequently included artefacts from the cingulum bundle.

The study of this cleaning process can better inform the placement of exclusion ROIs in future studies for the sake of efficiency. For instance, in light of the maps shown in Figure 3C, it seems convenient to include the temporal ROI used for the lAF as an exclusion region for the aAF. Further, a ROI

between hemispheres can automatically discard all streamlines commonly merged with commissural fibres. Finally, insular connections were often dissected along with the AF, IFOF and UF, motivating a systematic placement of yet another "NOT" ROI.

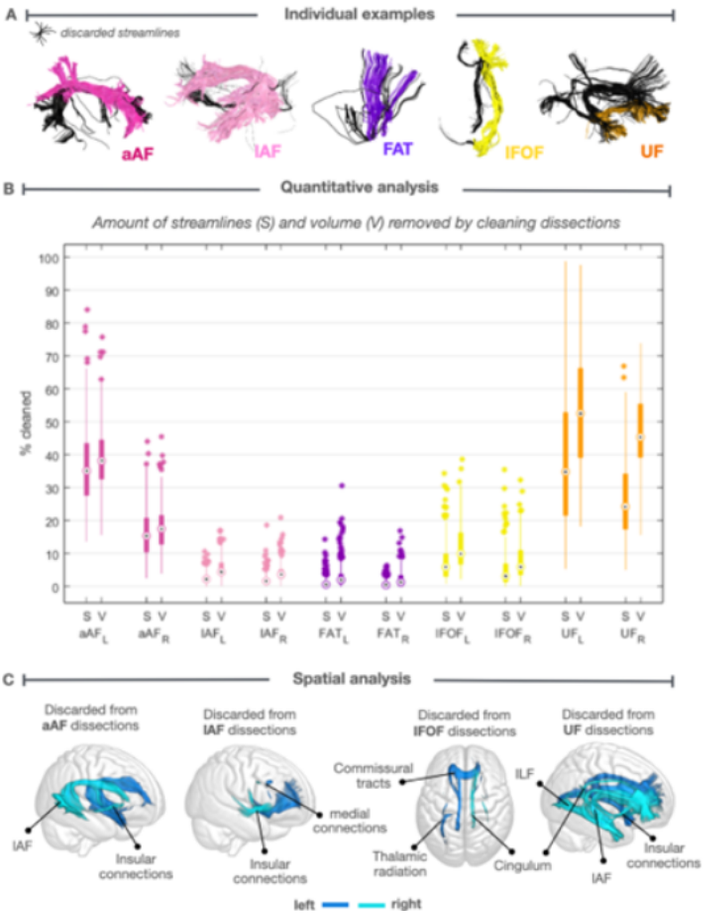

Figure 3: Manual cleaning of tractography dissections: quantitative and spatial analysis

Note: Quantitative and spatial analysis of the effect of manual cleaning of individual spherical deconvolution tractography dissections. A) individual examples of discarded streamlines (black). B) quantification of the percentage of streamlines (S) and volume (V) removed from the tract dissections during the cleaning process by exclusion ROIs. C) overlap map of voxels no longer present in visitation maps (>10% of individuals) after cleaning. The FAT contained no voxels fulfilling this criterion. aAF: anterior segment of the arcuate fasciculus, lAF: long segment of the arcuate fasciculus, FAT: frontal aslant tract, IFOF: fronto-occipital fascicle, UF: uncinate fasciculus, IFL: inferior longitudinal fasciculus.

With the final dissections, we were able to map the group effects of white matter connectivity of the language network. Figure 4 displays the effect size of voxels significantly present in the sample dissections according to a permutation-based one-sample t-test (voxel-wise family-wise error corrected). These maps form a probabilistic atlas of the frontal tracts of the language network and highlight the

robustness of the core of the tracts and hint at the span of each tract's terminations, which we later further explored. Some asymmetries are clearly visible, with the aAF reaching more inferior areas of the frontal lobe together with the MFg, and having a larger core in the right hemisphere. The lAF reaches the inferior and middle gyri of the frontal lobe, and has a branch reaching the precentral gyrus in the left hemisphere. On the other hand, the FAT and IFOF appear quite symmetric in shape and size of their core and branches. Finally, the right UF shows a larger core area but lacks the branch reaching the pars triangularis and stops at a more inferior part of the superior frontal gyrus (SFg) than in the left hemisphere.

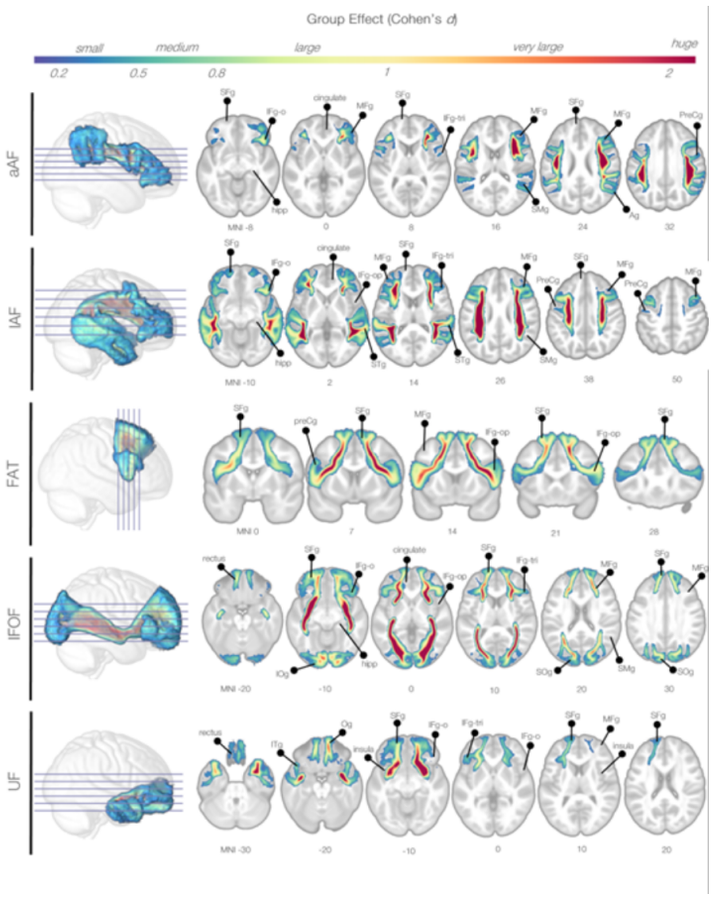

Figure 4: Effect size maps of language network tracts

Note: Group effect size maps (Cohen's *d*) of significant voxels according to a one-sample t-test (voxel-wise corrected for family-wise error). Slices are displayed in neurological convention. aAF: anterior segment of the arcuate fasciculus, lAF: long segment of the arcuate fasciculus, FAT: frontal aslant tract, IFOF: fronto-occipital fascicle, UF: uncinate fasciculus.

3.2 Interindividual Variability in White Matter Tracts

Interindividual variability was inspected in the tracts as well as their cortical terminations. Although group effect size maps indirectly measure interindividual variability, it is better elucidated by percent-

age overlap maps (Figure 5) that show that the FAT is the most spatially variable tract in the group while exhibiting the least spatial laterality. Such laterality was explored at the macro and microstructural levels through one-sample t-test analyses (Figure 6A), revealing a high degree of macrostructural (streamline count and volume) left-sided laterality of the lAF and right-sided laterality of the aAF and the UF. On the other hand, microstructural metrics such as HMOA, AP and FA are generally left-lateralised in the frontal language network. No significant sex effect was evident with an ANOVA analysis.

Histograms of the distribution of the left and right side metrics are provided in Figure 6C, where factors such as skewness and kurtosis of these metrics can be visualised. A systematic left-sided asymmetry in AP is clearly visible. Additionally, UF streamline count laterality can be explained by a higher proportion of individuals having a low streamline count rather than a shifted distribution, as is the case with the aAF.

From these histograms, it is not apparent which distributions have more or less variance. A Brown-Forsythe test indicates that the variability in the streamline count of aAF ($F(1, 394) = 37.36, p < .0001$) and the volume of the UF ($F(1, 394) = 30.42, p < .0001$) are significantly different in the left and right hemisphere (Figure 6B): higher variability in the right hemisphere for aAF and the left hemisphere for UF.

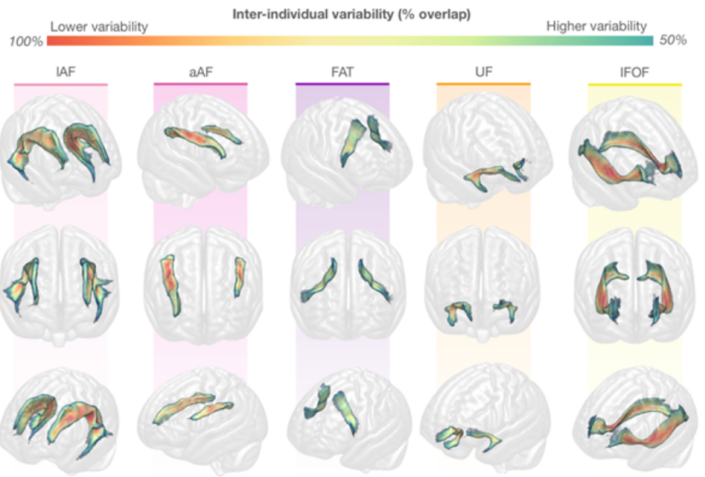

Figure 5: Interindividual variability of white matter tracts

Note: Interindividual variability reflected by a >50% overlap in dissections. Except for the FAT, most tracts contain a core of near 100% overlap among participants. aAF: anterior segment of the arcuate fasciculus, lAF: long segment of the arcuate fasciculus, FAT: frontal aslant tract, IFOF: fronto-occipital fascicle, UF: uncinate fasciculus.

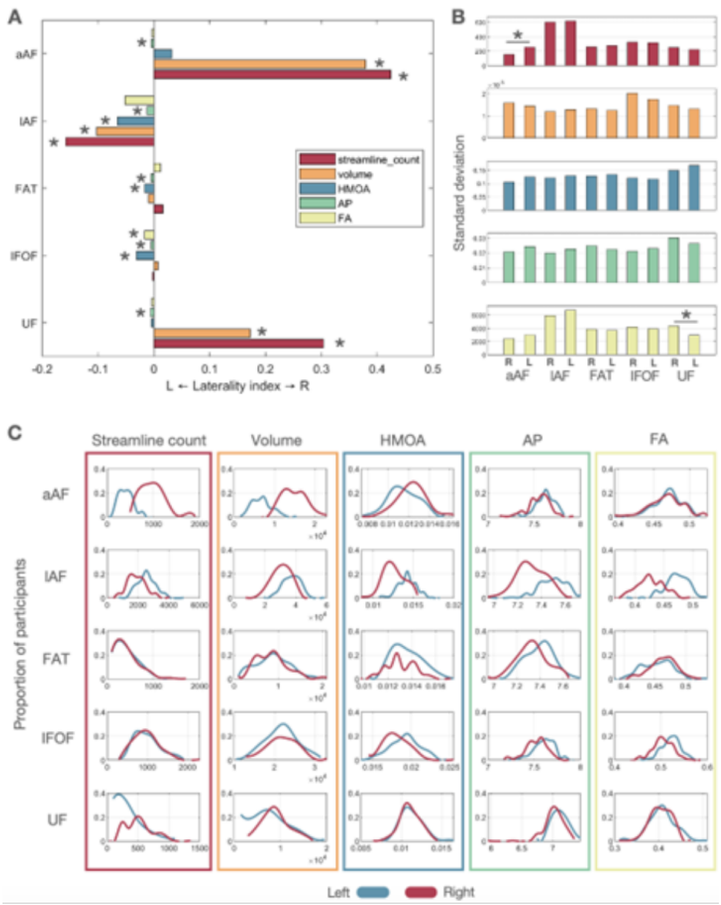

Figure 6: Variability and asymmetry across tracts and metrics

Note: (A) Laterality index for each tract across all metrics. Asterisks indicate Bonferroni-corrected significance of a one-sample t-test. (B) Standard deviation of each tract and metric. Asterisks indicate Bonferroni-corrected significance of a Brown-Forsythe test comparing variance across hemispheres. (C) Smoothed histograms of the proportion of participants for each metric value in left (blue) and right (red) hemisphere tracts. aAF: anterior segment of the arcuate fasciculus, lAF: long segment of the arcuate fasciculus, FAT: frontal aslant tract, IFOF: fronto-occipital fascicle, UF: uncinate fasciculus, HMOA: Hindrance Modulated Orientational Anisotropy, AP: anisotropy power, FA: fractional anisotropy.

3.3 Interindividual Variability in Cortical Terminations

Cortical projections were successfully computed for all tracts and participants, rendering effect size maps (Cohen's *d*) and allowing for the computation of a laterality index with the smoothed and binarised termination points (Figure 7). Additionally, this figure displays the results of a one-sample t-test on the laterality indexes, Bonferroni corrected to an alpha of 0.01.

Exclusively considering the frontal lobe, we see an almost complete bilateral coverage by the composite of the 5 tracts. The surface area of frontal termination of the aAF is significantly right-lateralised

($t(197) = 20.07, p < .001$) and more consistently reaches anterior portions of the inferior and middle frontal gyrus on the right hemisphere, but we see a lower group effect of the terminations in the precentral gyrus. Similarly, in the case of the long segment, connectivity to the precentral gyrus (middle portion) is only present in the left hemisphere. The area of coverage and the pattern of effect size are asymmetric, with the left hemisphere containing more termination points ($t(197) = -26.51, p < .001$) and two clusters of high effect size (inferior frontal juncture and anterior IFg). The remaining dorsal tract, the FAT, had two frontal termination areas, the posterior superior frontal gyrus or supplementary motor area, and the inferior frontal gyrus, specifically the par opercularis and triangularis. Although less apparent in the effect size maps, the FAT had a significantly negative laterality index ($t(197) = -15.22, p < .001$), meaning the left side more consistently had a wider termination area than the right at the individual level.

The two dissected ventral tracts, the IFOF and the UF, merge their paths at a bottleneck high-density area, the external capsule. This boosts the chance of erroneous tracking where a UF streamline may merge with an IFOF streamline and generate false positives and negatives in the frontal terminations (Liakos et al., 2021). Hence, the following results are to be interpreted with this in mind. In contrast to the previous tracts, the IFOF termination area is symmetric ($t(197) = -2.01, p = .046$) and of very high and homogeneous effect size, mainly highlighting the anterior portion of the superior frontal gyrus, the frontal pole, and the pars orbitalis and triangularis. Asymmetry, in this case, is only noted in the right-lateralised effect size attributed to these last two termination areas. In comparison, a shift of effect size towards more orbital areas is appreciated for the UF, while still reaching the anterior SFg in the left hemisphere. The variability of the laterality index is the highest for this tract, while still having a significantly positive mean ($t(197) = 3.45, p < .001$).

Overall, the asymmetry of the frontal language network terminations in the healthy brain is highly notable, with varying effect size patterns and area of coverage. The termination laterality indexes follow those of volume and streamline count except for the FAT, which was not shown to be left lateralised based on the tract-based measures (Figure 7). Since the whole of the FAT's volume belongs in the frontal lobe, this difference was unexpected and prompted the creation of a linear model with volume laterality as a predictor and whole-brain termination laterality as the outcome. The intercept was significantly negative (indicating leftwards laterality) for all tracts: aAF ($B = -.11, SE = .02, t(196) = -4.57, p < .001$), lAF ($B = -.17, SE = .01, t(196) = -20.25, p < .001$), FAT ($B = -.29, SE = .01, t(196) = -22.13, p < .001$), IFOF ($B = -.04, SE = .01, t(196) = -5.42, p < .001$) and UF ($B = -.04, SE = .01, t(196) = -2.94, p = .004$). Similar results were obtained using streamline count as the predictor in the linear model: aAF ($B = -.08, SE = .03, t(196) = -2.92, p = .004$), lAF ($B = -.16, SE = .01, t(196) = -16.89, p < .001$), FAT ($B = -.30, SE = .01, t(196) = -22.93, p < .001$), IFOF ($B = -.03, SE = .01, t(196) = -3.20, p < .001$) and UF ($B = -.12, SE = .02, t(196) = -6.86, p < .001$). This points to a systematic larger fanning out of the streamlines near the cortex in the left hemisphere since in the absence of volume or streamline count laterality, we would still find a larger termination area in the

left hemisphere for all tracts, but especially the FAT.

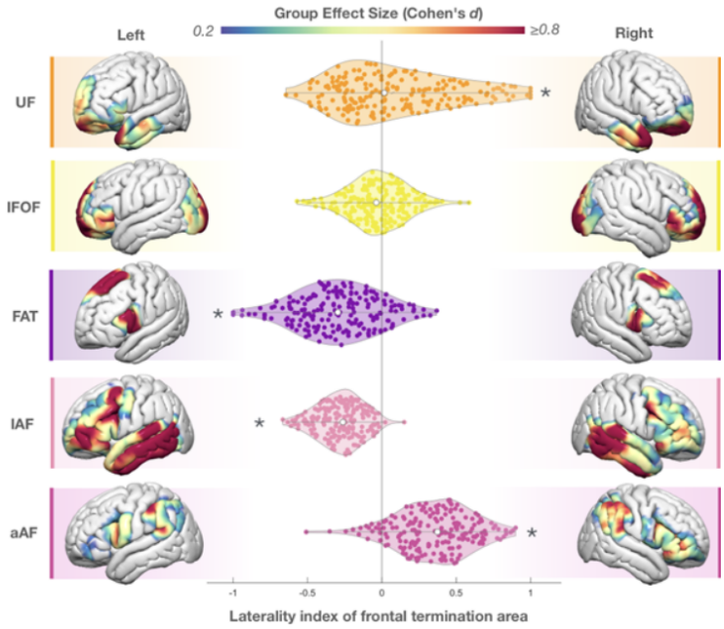

Figure 7: Topography and laterality of the frontal terminations of the language network

Note: Termination maps in the cortical surface reflect group effect size (Cohen's *d*), with hemispheric asymmetries in both the variability patterns and the extent of cortical area that tracts reach. Violin plots showcase the laterality index computed with the area of coverage of a tract in each frontal lobe individual. Asterisks indicate one-sample t-test significance (Bonferroni corrected). aAF: anterior segment of the arcuate fasciculus, lAF: long segment of the arcuate fasciculus, FAT: frontal aslant tract, IFOF: fronto-occipital fascicle, UF: uncinate fasciculus.

Termination Component Analysis

The termination distribution pattern of these tracts elucidates a significant variability as well as possible components, as discussed for the lAF. We applied an independent component analysis (ICA) to tease these terminations apart and describe such components. In order to whiten the data for a more accurate ICA, a PCA was performed on the binary maps of each individual's terminations. We can interpret the real data as composed of a linear combination of the extracted components in both types of analyses.

The first five principal components shown in Figure 8 explained up to 22% of the variance in the data (aAF: left 18.1%, right 14.2%; lAF: left 14.8%, right 13.7%; FAT: left 22.4%, right 22.1%; IFOF: left 16.1%, right 17.5%; UF: left 20.6%, right 20.4%). Most of the tracts show asymmetries in their principal components. In the case of the aAF, the left side shows more homogeneous and clustered patterns of termination than the right. Similarly, the left lAF is somewhat more organised and shows a posterior to anterior directionality whereas a mixed or inferior-superior directionality is more pronounced

in the right hemisphere. Since the FAT is an intra-lobular tract, its principal components must be interpreted slightly differently, knowing that a termination point in the IFg always corresponds with another in the SFg, and these pairwise patterns are more likely to be the ones explained. A similarity between the two hemispheres is the correspondence of posterior and anterior sections of the two termination areas, showing that although the path is not a straight line, the degree to which fibres cross in this direction is small. Additionally, similar bilateral patterns may appear, as is the case of the left C4 and right C2 of the IFOF terminations. They both highlight the terminations to Broca's area, but the ordering is different, highlighting what we could already see in Figure 7 regarding the effect size asymmetry in this area. Finally, the UF components highlight clusters including the orbitofrontal cortex, IFg and SFg.

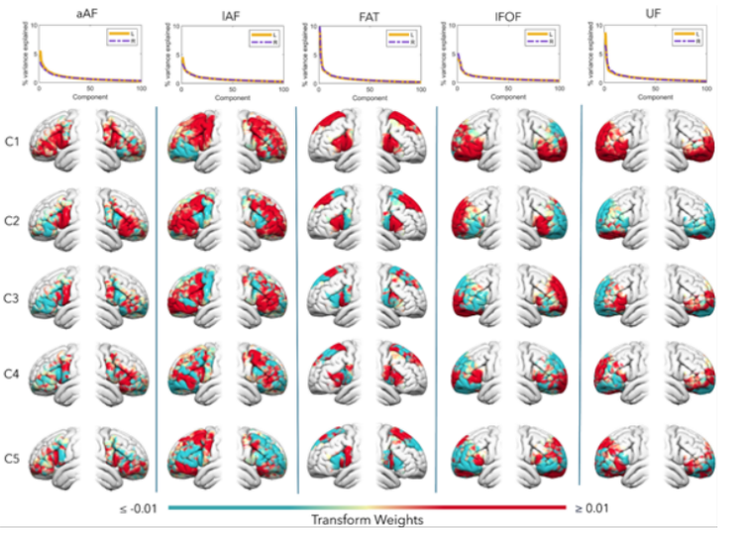

Figure 8: Patterns of frontal terminations: Principal Component Analysis (PCA)

Note: First 5 principal components of the frontal terminations are depicted in rows and variance explained with the first 100 components is depicted at the top. aAF: anterior segment of the arcuate fasciculus, lAF: long segment of the arcuate fasciculus, FAT: frontal aslant tract, IFOF: fronto-occipital fascicle, UF: uncinate fasciculus.

In summary, right-hemisphere patterns appear to be generally less organised and hence more heterogeneous. The order of the principal components highlights the main sources of variability in the cortex and these are sometimes different across hemispheres.

Using the first 50 principal components, we derived 5 independent components and plotted the combined transformation weights onto the surface (Figure 9). The extent to which a pattern or component is present in an individual's terminations is reflected in their component score (violin plots in Figure 9). Such score is obtained by multiplying the weight of each vertex by the corresponding value for a given participant. Hence, high negative scores reflect the importance of the component but in its inverted form. Scores around the origin indicate that the pattern is not expressed in a participant.

In the case of ICA, components are not ordered, but kurtosis —a measure of non-gaussianity— can be used to rank the components in terms of statistical independence (Figure 9). Independent components of the aAF are noisy but mainly highlight the independence of motor and inferior frontal terminations in the left hemisphere, which is not so defined in the right. More asymmetries are present in the lAF terminations, where patterns of left posterior-anterior and slight right inferior-superior directionality of change that were already visible with the PCA, survive the independence test of ICA. Additionally, the fourth component seems to segment Broca's area into its components of Broadman's area 44 and 45. After the ICA weights are added to the previous principal component maps, FAT is more clearly sectioned, pointing to a potential opportunity for segmentation based on termination areas. The relationship between its inferior and superior termination is also asymmetric, with examples as the fourth component (C4) that segments the inferior projections into the precentral gyrus and IFg, while the corresponding separation of the superior terminations is not mirrored across hemispheres.

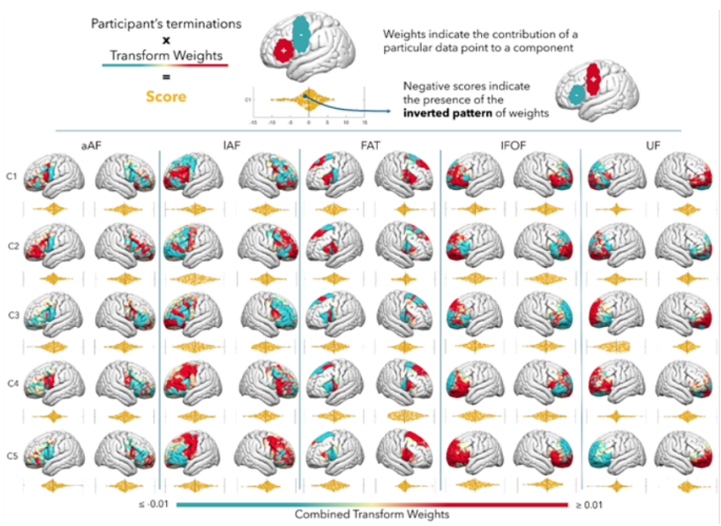

Figure 9: Patterns of frontal terminations: Independent component analysis (ICA)

Note: Independent component analysis (ICA) was performed on whitened data consisting of the first 50 principal components of binary termination maps. Combined transformation weights (PCA ICA) show the contrasting areas that contribute to a component. Violin plots indicate the distribution of component scores across participants. The score is the result of multiplying the data and weighting, elucidating how present a given pattern is in an individual. Participants close to the vertical line of the violin plot (zero) exhibit little of that component, while those at the left (negative scores) exhibit the inverted pattern to the one shown. ICA component weights are ordered by kurtosis, a measure of non-gaussianity that indicates higher statistical independence. aAF: anterior segment of the arcuate fasciculus, lAF: long segment of the arcuate fasciculus, FAT: frontal aslant tract, IFOF: fronto-occipital fascicle, UF: uncinate fasciculus.

We then fed the component scores into UMAP to explore if a nonlinear representation of these in

an embedding space was able to cluster participants in terms of their full language network frontal termination components. No evident clustering was found in 2 nor 3 dimensions after parameter tuning.

3.4 Anatomical Relation to Behavioural Factor Scores

Efforts to relate anatomical features to the available behavioural scores were deemed non-significant after applying Bonferroni correction to the linear mixed effects models and the correlations to the independent components.

3.5 Validation of MegaTrack

When performing MegaTrack dissections, 800 tractograms were overlaid (200 participants, 2 modalities and 2 hemispheres). This greatly helped identify and quickly clear out major artefacts but also made the more fine-grained cleaning of the dissections more difficult, which is especially important in SD reconstructions since they are more prone to false positive streamlines. This level of detailed cleaning refers to being able to remove streamlines crossing sulci, looping back along the tract, or taking sharp angles still within the tracts trajectory. Hence, individual dissections are bound to be imperfect, but consistently so, meaning that what is discarded for one participant is discarded for all, including both reconstruction types and hemispheres. Additionally, dissections can be carried out in a matter of days instead of months. MegaTrack has previously undergone in-house validation with a small dataset, but was lacking a large-scale external validation.

We successfully retrieved all tracts in SD tractograms but found some to be missing when dissecting the DTI reconstructions (aAF: 1 left, 1 right; lAF: 1 left, 17 right; FAT: 16 left, 13 right; UF: 1 left). The difficulty to retrieve tracts such as the right lAF in DTI has been previously documented (S. J. Forkel, Thiebaut de Schotten, Dell'Acqua, et al., 2014).

In order to validate the use of MegaTrack against manual dissections in a large dataset we computed spatial similarity coefficients (Figure 10) as well as correlations of micro and macrostructural metrics (Table 1). While a Dice coefficient of 1 would indicate total overlap, we obtain coefficients around the 0.8 mark, indicating high spatial agreement between dissection methods. Additionally, we see a slight trend of right hemisphere tracts exhibiting higher spatial overlap than their counterpart (Figure 10). In terms of metric correlation, MegaTrack dissections exhibit a similar distribution of values, especially consistent for the volume metric (Table 1).

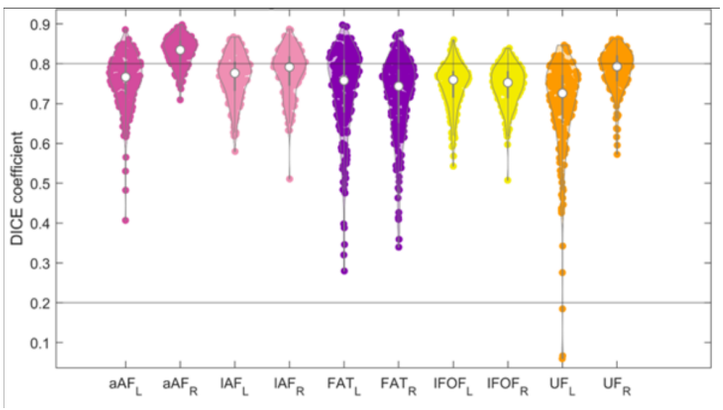

Figure 10: MegaTrack validation: spatial similarity between manual and MegaTrack SD dissections

Note: Dice coefficient of similarity of the visitation maps of MegaTrack and manual dissections of SD tractograms. There is overall agreement, especially for right hemisphere tracts. aAF: anterior segment of the arcuate fasciculus, lAF: long segment of the arcuate fasciculus, FAT: frontal aslant tract, IFOF: fronto-occipital fascicle, UF: uncinate fasciculus.

Table 1: Spearman correlation between metrics obtained from MegaTrack and manual SD dissections

Tract	Hemisphere	Metric	ρ	p
Arcuate Fasciculus Anterior Segment (aAF)	Left	Streamline count	0.90	$< .001$
		Volume	0.90	$< .001$
		HMOA	0.81	$< .001$
		AP	0.78	$< .001$
		FA	0.86	$< .001$
	Right	Streamline count	0.70	$< .001$
		Volume	0.76	$< .001$
		HMOA	0.75	$< .001$
		AP	0.80	$< .001$
		FA	0.86	$< .001$
Arcuate Fasciculus Long Segment (lAF)	Left	Streamline count	0.64	$< .001$
		Volume	0.71	$< .001$
		HMOA	0.62	$< .001$
		AP	0.78	$< .001$
		FA	0.82	$< .001$
	Right	Streamline count	0.66	$< .001$
		Volume	0.81	$< .001$
		HMOA	0.81	$< .001$
		AP	0.81	$< .001$
		FA	0.84	$< .001$

Tract	Hemisphere	Metric	ρ	p
Frontal Aslant Tract (FAT)	Left	Streamline count	0.92	$< .001$
		Volume	0.91	$< .001$
		HMOA	0.67	$< .001$
		AP	0.82	$< .001$
		FA	0.87	$< .001$
	Right	Streamline count	0.91	$< .001$
		Volume	0.85	$< .001$
		HMOA	0.68	$< .001$
		AP	0.83	$< .001$
		FA	0.89	$< .001$
Inferior Fronto-Occipital Fasciculus (IFOF)	Left	Streamline count	0.83	$< .001$
		Volume	0.89	$< .001$
		HMOA	0.70	$< .001$
		AP	0.78	$< .001$
		FA	0.86	$< .001$
	Right	Streamline count	0.71	$< .001$
		Volume	0.82	$< .001$
		HMOA	0.73	$< .001$
		AP	0.75	$< .001$
		FA	0.84	$< .001$
Uncinate Fasciculus (UF)	Left	Streamline count	0.96	$< .001$
		Volume	0.98	$< .001$
		HMOA	0.84	$< .001$
		AP	0.82	$< .001$
		FA	0.91	$< .001$
	Right	Streamline count	0.91	$< .001$
		Volume	0.92	$< .001$
		HMOA	0.86	$< .001$
		AP	0.81	$< .001$
		FA	0.91	$< .001$

Note: SD: Spherical Deconvolution, HMOA: Hindrance Modulated Orientational Anisotropy, AP: anisotropy power, FA: fractional anisotropy.

3.6 Methodological Variability in Tracts and Terminations

The use of MegaTrack allowed for the comparison of results stemming from tracts dissected simultaneously for both hemispheres and two reconstruction methods, hindering the possibility of rater bias while standardising the process. Comparing the laterality indexes of the SD MegaTrack dissections with those of the manual dissections we can see if some laterality was introduced by the person

performing manual cleaning of each individual brain and hemisphere. After fitting a linear model with MegaTrack dissections as the predictor and the manual dissections as an outcome, we obtain a significant effect of the intercept for several tracts in terms of streamline count (aAF: $B = .12, SE = .02, t(196) = 7.56, p < .001$; UF: $B = .10, SE = .01, t(196) = 7.95, p < .001$) and volume (aAF: $B = .07, SE = .01, t(196) = 4.97, p < .001$; FAT: $B = .03, SE = .01, t(196) = 3.55, p < .001$; UF: $B = .08, SE = .01, t(196) = 11.67, p < .001$). This means that with no laterality in MegaTrack dissections we would still record positive (right-sided) laterality in these tracts. Naturally, the scale of the intercepts should be noted together with the values of mean laterality to assess their proportional relevance.

Additionally, we established that the type of reconstruction will largely affect the dissection results because of the ability to resolve crossing fibres (streamline false negatives and positives). We measured the similarity of the visitation maps using the Dice coefficient of similarity (Figure 11). Our results indicate that the ventral tracts, IFOF and UF, are consistently similar between reconstruction methods, while the dorsal tracts show a wide variability.

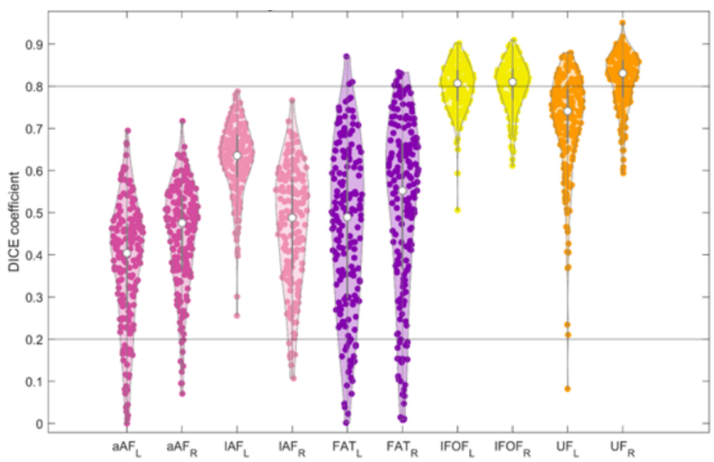

Figure 11: Spatial similarity between DTI and SD dissections performed simultaneously using MegaTrack

Note: Dice coefficient of similarity of the visitation maps of MegaTrack dissections of DTI and SD performed simultaneously for each tract. The ventral IFOF and UF show more consistency and agreeance between reconstruction methods while the dorsal tracts exhibit a wide range of variability of the dissection result depending on the reconstruction method. DTI: diffusion tensor imaging, SD: spherical deconvolution, aAF: anterior segment of the arcuate fasciculus, lAF: long segment of the arcuate fasciculus, FAT: frontal aslant tract, IFOF: fronto-occipital fascicle, UF: uncinate fasciculus.

To infer the effect of the choice of reconstruction method in measuring asymmetries, we plotted the laterality indexes of micro and macrostructural metrics for each of these methods when using MegaTrack to dissect them at the same time for both reconstruction types and hemispheres (Figure 12). Using DTI, the laterality of the lAF becomes enhanced while it decreases for aAF. The FAT now also exhibits right sided laterality.

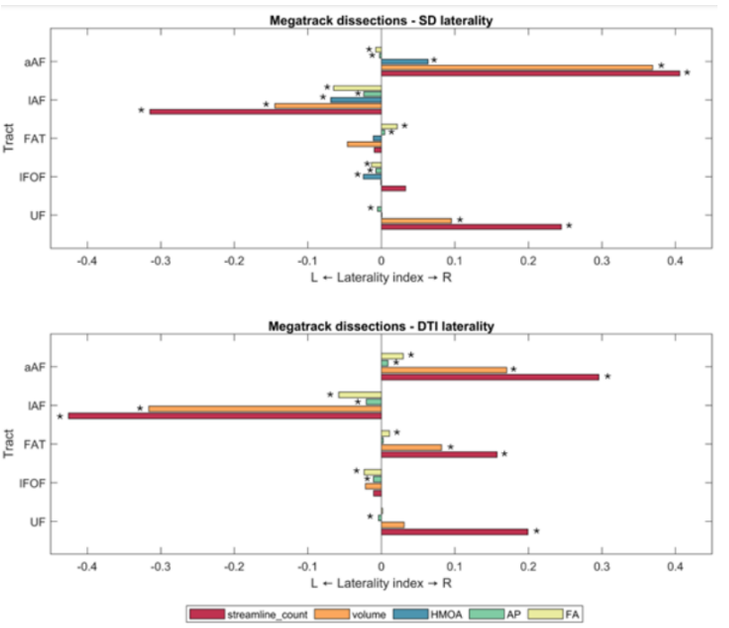

Figure 12: Differences in laterality indexes in dissections of DTI and SD reconstructions

Note: Laterality indexes for micro and macrostructural metrics in MegaTrack dissections of DTI and SD tractography performed simultaneously for both modes of reconstruction as well as both hemispheres. Asterisks represent statistical significance of a one-sample t-test after Bonferroni correction. DTI: diffusion tensor imaging, SD: spherical deconvolution, aAF: anterior segment of the arcuate fasciculus, lAF: long segment of the arcuate fasciculus, FAT: frontal aslant tract, IFOF: fronto-occipital fascicle, UF: uncinate fasciculus, HMOA: Hindrance Modulated Orientational Anisotropy, AP: anisotropy power, FA: fractional anisotropy.

When comparing the termination areas and patterns of effect size in DTI and SD (Figure 13), aAF terminations are highly variable in SD but show a strong interindividual agreement in DTI in the precentral gyrus. For lAF in DTI we see a similar pattern with tracts preferentially terminating within the posterior frontal lobe while the SD maps show more variable and forward-reaching dissections toward the pars tringularis, opercularis and orbitalis. In the case of the FAT, only the area of termination in the SFg is different, with a pattern that favours the more ventral portion of the SFg in DTI in contrast to a coverage of the whole gyrus in SD. Both the IFOF and UF show a more consistent termination in Broca's area (BA 44 and 45) in the DTI maps, while SD more often describes streamlines reaching the SFg in the IFOF.

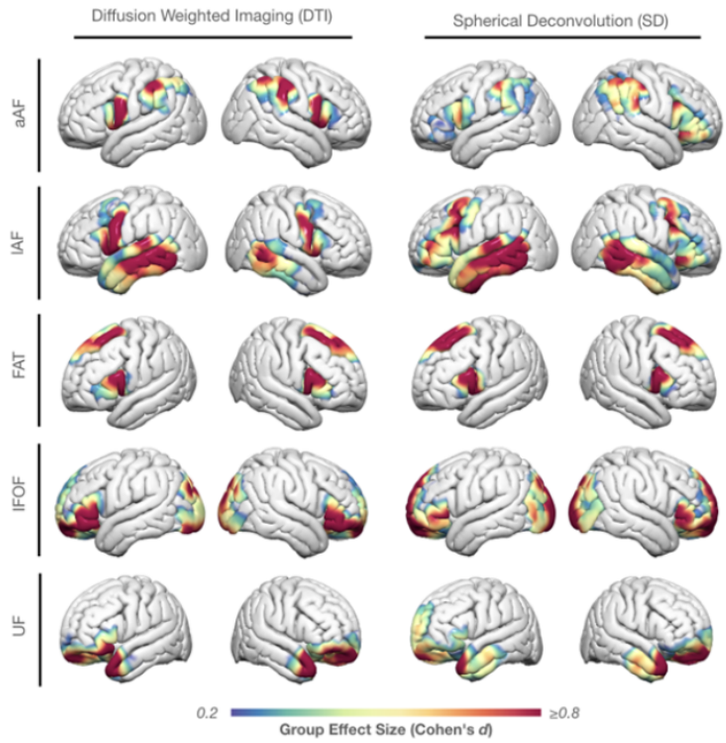

Figure 13: Effect size of cortical terminations in DTI and SD dissections performed with MegaTrack

Note: Effect size (Cohen's *d*) of cortical terminations of DTI and SD dissections performed simultaneously for both reconstruction types and hemispheres to avoid rater bias. aAF: anterior segment of the arcuate fasciculus, lAF: long segment of the arcuate fasciculus, FAT: frontal aslant tract, IFOF: fronto-occipital fascicle, UF: uncinate fasciculus.

4 Discussion

This study represents a multi-level effort to map and describe the variability and extent of the terminations of the language network in the frontal lobe. Our results showed that i) the language network is highly variable and asymmetric, favouring both the right and left hemisphere in different instances, ii) there are cortical reach asymmetries beyond volumetric and metric-wise asymmetries, iii) an individual's frontal terminations can be partially described in terms of independent components, and iv) the choice of reconstruction method drastically alters detected asymmetries and termination patterns even when dissected simultaneously with the same constrictions. We subsequently discuss these results in detail.

Our first result indicates that interindividual variability governs spatial and microstructural aspects of language anatomy. We started exploring interindividual variability and laterality of the tracts, which showed an overall leftward asymmetry for the lAF, FAT and IFOF, and rightward asymmetry for the aAF and UF. These results largely confirm previous studies (Thiebaut de Schotten et al., 2011). Several exceptions were presented, however. While the direction of laterality for aAF (rightward asymmetry) and lAF (leftward asymmetry) aligned, the index of laterality for streamline count and volume

was approximately double in our aAF but a quarter in our lAF. Additionally, Thiebaut de Schotten and colleagues observed right-sided laterality in the IFOF for streamline count, which is at odds with our results, while we observed left-sided FA laterality for the IFOF that was not significant in their sample. Lastly, we obtained high right-sided laterality for the uncinate fasciculus for streamline count and volume - neither of which was shown in the previous study. This difference in UF laterality findings is a common observation and has hindered a definite description of its laterality so far (Ocklenburg et al., 2016). Overall, our study relied on a large sample of nearly 200 volunteers, while most previous work was conducted on smaller samples (e.g. Catani Thiebaut de Schotten (2008), n=12; Thiebaut de Schotten et al. (2011), n=40). In addition, most previous work focussed on measures of volume, FA, and streamline count (Catani and Thiebaut de Schotten, 2008; Thiebaut de Schotten et al., 2011), while we included further indices (e.g. HMOA and AP). For the interindividual variability explored through percentage overlap maps, our dissections rendered larger overlap areas for aAF, lAF, and IFOF but similar ones for UF (Thiebaut de Schotten et al., 2012). These spatial differences were expected, since Thiebaut de Schotten et al. employed a DTI reconstruction method, which is less able to resolve crossing fibres and typically visualises the core of a tract rather than its full extent as with Spherical Deconvolution. This fundamental difference might also account for some laterality differences, given that the predominance of the aAF is mainly reflected in more frontal reaching fibres that are commonly not observed with DTI, leading to a lower laterality index in DTI. Additionally, it is common with DTI to have difficulty dissecting the right lAF, which can be completely absent in some participants (Catani et al., 2007; S. J. Forkel, Thiebaut de Schotten, Dell'Acqua, et al., 2014). While a similar grading of the right arcuate fasciculus can be observed using the SD algorithms, the extreme cases of no right arcuate fasciculus are rare, naturally leading to a lower left volume and streamline count laterality indexes. Using the MegaTrack software, we corroborated this issue of missing tracts and verified that computing laterality indexes with DTI reconstruction (Figure 12) rendered values closer to the ones reported by Thiebaut de Schotten et al. (Thiebaut de Schotten et al., 2012). Using MegaTrack, we did, however, observe missing left FAT dissections in DTI in 9% of the participants. This observation contributed to a stronger right-sided streamline and volume laterality that is at odds with the established literature (Catani et al., 2013). Overall, these methodological considerations contribute to the observed anatomical differences.

Further, the impact of methodological variability on tractography reconstruction and dissection was analysed by Schilling et al. (Schilling et al., 2021) who gathered dissections performed on the same preprocessed data from 42 independent teams around the globe. Their analysis showed that variability across dissection protocols is greater than all other sources of variability in the dissections, including interindividual variability. This study also showed the relevance of anatomically informed methods to avoid artefactual reconstructions. As such, this study calls for the implementation of good practices that we tried to prioritise in our study, including offering transparency in the choice of ROIs and dissection protocol (see Figures 2 and 3) and exploring quantifying intra-protocol variability (performed by comparing variability in MegaTrack vs. manual). In particular, our novel approach to

measuring this methodological variability made it possible to not only estimate differences between and within reconstruction methods (complementary to the study by Schilling et al. (2021)), but also differences in laterality results when the dissection was blind to such laterality effects. Fitting a linear model with MegaTrack as an unbiased predictor of the laterality index of manual dissections, we obtain a significantly positive intercept for some of the tracts, meaning that in the absence of laterality in the MegaTrack dissections, we would still find right laterality in the manual dissections. This points to a potential rater bias but could also be explained by a higher density of obscured artefacts in the left hemisphere that were better cleaned in the one-by-one cleaning process. The size of this effect, though, is relatively small —with mean laterality indexes as high as 0.4 and high variability, a potential "bias" of around 0.1 might not be a concern.

This is the first study to externally validate and compare MegaTrack to manual dissections in a large dataset. A few learning points we observed in the process are the following: The density of the generated mega-tract forces the cleaning to be focused more on the overall shape than the individual streamlines. This is reflected in the correlations with manual metrics, where volume is more consistently correlated than streamline count. The latter has often been criticised as a metric given the disconnection to the true anatomy (Jones, 2003). Overall, MegaTrack rendered dissections highly similar to the manual dissections in volume and space, rendering it a time-efficient alternative for large datasets and studies with an interest in white matter segmentation. More care might be required for the study of the terminations since fine-grain cleaning allows for the detection of spurious streamlines crossing over sulci or with an anatomically implausible trajectory within the normal bound of the tract. This is harder to achieve with MegaTrack when dissecting a large bilateral and bimodal mega-tract and this was reflected in slightly more variable termination maps (Figures 7 and 13).

When focussing on the tract terminations, we face the problem of higher noise because of a lower diffusion signal near the cortex, and the added layers of abstraction and processing needed to translate streamline information to the cortex. With these caveats in mind, we still find differences in the laterality of terminations and tracts, especially puzzling for the FAT, an intralobular tract with no significant volume or streamline count laterality but high left-sided laterality of the terminations. This prompted further whole-brain regression analyses of volume and termination laterality. A significant negative intercept for all tracts pointed to systematic hemispheric differences in the fanning of tracts near the cortex, rendering a larger surface of termination in the left hemisphere even in the absence of volume laterality. In sum, our analysis was able to characterise asymmetries in whole-brain cortical reach favouring the left hemisphere beyond those detectable by volumetric differences, which was most notable for the FAT but significant for the whole set of 5 language tracts.

More asymmetries were highlighted by the group effect size maps of the tract terminations in terms of the area of coverage and the patterns of effect size. Generally, terminations to the precentral gyrus were more prominent in the left hemisphere and the aAF was the only tract without an area of high effect size in the frontal lobe, indicating higher variability of termination areas. When comparing

DTI and SD terminations from MegaTrack dissections, this was no longer the case in DTI, and a clear pattern of more forward-reaching tracts in SD was present. Conversely, DTI dissections more consistently terminated in the same areas, often involving the precentral gyrus in arcuate fasciculus dissections, and more strongly highlighting the pars orbitalis and triangularis (part of Broca's area) in IFOF and UF terminations. Overall, DTI tracts tend to stop at shorter distances and have more consistent terminations, which can be linked back to the methodological bias to primarily reconstruct the core of the tract with lower variability (Rojkova et al., 2016).

In manual SD dissections of the UF, we noted SFg terminations in the left hemisphere. These have been discarded by some post-mortem studies (Liakos et al., 2021), while several imaging studies include them. Weiller et al. (Weiller et al., 2021) argued for the existence of a continuous ventral tract composed of the UF and IFOF. Given the location of the UF in an area especially prone to imaging artefacts, the merging of UF and IFOF streamlines in the frontal lobe after the bottleneck passageway in the extreme capsule might represent a methodological limitation. However, we wondered about the source of the laterality of this effect. Since such an effect was reproduced in the MegaTrack dissections, which are blinded to the hemispheric side, ensuring left and right are cleaned in the same way, it seems we captured a systematic effect in the data rather than one stemming from inconsistencies in the manual cleaning. Future work should review the literature and use a multimethodological approach, combining anatomical, functional and lesion approaches, to define the UF anatomy in relation to the SFg.

We applied principal component analysis (PCA) and independent component analysis (ICA) to gain a deeper understanding of the patterns that constitute the frontal terminations. Here, more asymmetries were uncovered, referring to the directionality of the pattern as well as the ordering of similar components in each hemisphere. A notable result was that the FAT components were cleaner and organised in such a way that prompts a possible alternative to prior attempts of FAT segmentation (Varriano et al., 2020), in this case, based on the independent components of cortical projections. Future work might investigate the FAT in terms of its stratification across the frontal lobe and the possible functional roles of its branches.

To explore the importance of the components and anatomical measures of the frontal white matter in explaining language function, we associated them to behavioural measures. Our results indicated that the termination patterns and white matter metrics were not directly related to the summative linguistic factor scores. One possible explanation might be that both the component scores and the factor scores are highly processed variables, far removed from the raw data, making it difficult to establish a linear relationship over all the layers of abstraction. Therefore, using raw behavioural scores may offer additional nuances in the future.

Overall, our study focused not only on the degree of interindividual variability and hemispheric asymmetry but also on the specific patterns of this variability, especially regarding the topography of frontal terminations. We sought to determine whether typical termination patterns exist that could charac-

terise an individual's unique neural profile. While we identified certain patterns, they account for only a small percentage of the observed variability and do not classify individuals into distinct phenotypes. The complexity and extent of variability in tract terminations were too great to be neatly categorised, even using advanced dimensionality reduction techniques such as UMAP. This finding underscores the challenge of capturing the full scope of anatomical diversity in the brain, highlighting the need for more nuanced approaches in neuroanatomical research. Efforts should be undertaken in the future to map these patterns as a valuable baseline for studying termination disruptions in language-related disorders as well as offer a new perspective for the study of the historical evolution of anatomical connections in the frontal lobe (Barrett et al., 2020; Thiebaut de Schotten et al., 2012).

4.1 Future Directions

We took a novel approach to investigate the anatomical foundation of the language network within the frontal lobe. Based on our results several future directions emerged.

A key aspect of the relevance of these results lies in their integration and comparison with the preceding body of literature looking at the tractography of these language tracts and zooming into their projections. To this end, we initiated a systematic review. An abstract and full-text screening of an initial set of 1254 articles resulted in a shortlist of 197 articles that will soon undergo data extraction based on shown or reported tractography terminations of the language tracts terminating in the frontal lobe. This work will address several questions raised by this current work, such as the FAT segregation or the UF's SFg projections.

Future research could combine macrostructural anatomy, such as tractography termination areas, with microstructural measures of the cortex, such as cytoarchitecture or receptoarchitecture. International initiatives are currently mapping the latter in 3D atlases (github-pages.ucl.ac.uk/NextBrain, Casamitjana et al., 2024; ebrains.eu/tools/siibra-explorer, Dickscheid et al., 2024; Amunts et al., 2024) and uncovering differences in interindividual variability in BA 44 and 45 that may affect functions beyond language (Amunts et al., 1999; Binkofski et al., 2000). Pairing these scales of variability might add explanatory power to functional and behavioural aspects of language.

At the macro scale, connectional anatomy and function can be jointly explored by projecting functional MRI (fMRI) data to white matter using methods such as the Functionnectome (Nozais et al., 2021; Nozais et al., 2023). Hence, fMRI tasks in the Language in Interaction (LiI) dataset could be analysed in the traditional way to obtain areas of cortical activation (fMRI) as well as determine the tracts involved in these tasks (functionnectome). Results from the present study can be related to those stemming from both these analyses to see if anatomical laterality corresponds with functional laterality of the tracts and cortical termination areas. This is of particular interest since clinical studies indicated that structural and functional variability play a pivotal role in language recovery after stroke (S. J. Forkel, Thiebaut de Schotten, Kawadler, et al., 2014; Saur et al., 2006). However, until now, there was no dataset available to systematically relate structure and function with linguistic

measures in a large enough sample. Going forward, we aim to use the available data from LiI to shed light on the relation between structure and function in the framework of language.

A natural continuation to our study would involve exploring the independent components of the tracts considering both their termination areas. We saw how ICA applied on the FAT rendered components more focused on paired terminations across main areas (SFg and IFg) given that it was an intralobular frontal tract. Such components pointed to a potential new way of segmenting the FAT that might also surface for other tracts if ICA is fed both their areas of termination.

Lastly, the frontal lobe is an area of significant evolutionary change that has experienced expansion and multi-level changes through the phylogenetic tree (Sherwood and Smaers, 2013; Smaers et al., 2010; Smaers et al., 2011). This, coupled with the addition of an extra temporal gyrus associated with language, prompt further consideration of comparative anatomical studies into the language network termination patterns across species.

4.2 Limitations

In this study, several limitations should be acknowledged that may affect the interpretation and generalisation of our findings. First, while tractography provides valuable insights into neural pathways, not all reproducible features are necessarily anatomically accurate (Zhang et al., 2022). Artefacts such as looping that prompt the exclusion of some streamlines can affect values like streamline count. Additionally, using factor scores for behavioural measures can introduce ceiling effects and reduce detail, limiting the granularity and sensitivity of these assessments. Regarding the component analysis, there is no standard guideline to assess the number of components that should be extracted, leading to a chance of choosing a suboptimal set. Finally, the reliance on binarised individual maps meant that we lost information about the density and distribution of streamlines and their terminations, which could have provided more nuanced insights into structural connectivity. These limitations suggest caution in interpreting the results and highlight areas for methodological improvements in future research.

5 Conclusion

Our study on connectional anatomy highlights the need for a reconceptualisation of language models, looking beyond the classical language areas and granting due importance to the full extent of the frontal terminations of the language network. Such endeavour is crucial to understand the network's integration with other cognitive functions. Although language is generally considered left-lateralised, anatomy nudges us to look further and consider the role of the right hemisphere. Asymmetries are prominent and vary across different levels of abstraction —from micro and macrostructural metrics to their area of cortical reach and pattern of termination. Such measurements are highly susceptible to methodological choices, hence it is essential to continue the pursuit of more accurate and reliable anatomical knowledge to inform our neurolinguistic and clinical models.

References

Amunts, K., Schleicher, A., Bürgel, U., Mohlberg, H., Uylings, H., & Zilles, K. (1999). Broca's region revisited: Cytoarchitecture and intersubject variability. *Journal of Comparative Neurology*, *412*(2), 319–341. https://doi.org/10.1002/(SICI)1096-9861(19990920)412:2<319::AID-CNE10>3.0.CO;2-7

Amunts, K., Axer, M., Banerjee, S., Bitsch, L., Bjaalie, J. G., Brauner, P., Brovelli, A., Calarco, N., Carrere, M., Caspers, S., et al. (2024). The coming decade of digital brain research: A vision for neuroscience at the intersection of technology and computing. *Imaging Neuroscience*, *2*, 1–35. https://doi.org/10.1162/imag_a_00137

Andersson, J. L., Graham, M. S., Drobnjak, I., Zhang, H., & Campbell, J. (2018). Susceptibility-induced distortion that varies due to motion: Correction in diffusion mr without acquiring additional data. *NeuroImage*, *171*, 277–295. https://doi.org/10.1016/j.neuroimage.2017.12.040

Andersson, J. L., Graham, M. S., Drobnjak, I., Zhang, H., Filippini, N., & Bastiani, M. (2017). Towards a comprehensive framework for movement and distortion correction of diffusion mr images: Within volume movement. *NeuroImage*, *152*, 450–466. https://doi.org/10.1016/j.neuroimage.2017.02.085

Andersson, J. L., Graham, M. S., Zsoldos, E., & Sotiropoulos, S. N. (2016). Incorporating outlier detection and replacement into a non-parametric framework for movement and distortion correction of diffusion mr images. *NeuroImage*, *141*, 556–572. https://doi.org/10.1016/j.neuroimage.2016.06.058

Andersson, J. L., & Sotiropoulos, S. N. (2016). An integrated approach to correction for off-resonance effects and subject movement in diffusion mr imaging. *NeuroImage*, *125*, 1063–1078. https://doi.org/10.1016/j.neuroimage.2015.10.019

Avants, B. B., Tustison, N. J., Song, G., Cook, P. A., Klein, A., & Gee, J. C. (2011). A reproducible evaluation of ants similarity metric performance in brain image registration. *NeuroImage*, *54*(3), 2033–2044. https://doi.org/10.1016/j.neuroimage.2010.09.025

Avants, B. B., Tustison, N. J., Stauffer, M., Song, G., Wu, B., & Gee, J. C. (2014). The insight toolkit image registration framework. *Frontiers in Neuroinformatics*, *8*. https://doi.org/10.3389/fninf.2014.00044

Barrett, R. L. C., Dawson, M., Dyrby, T. B., Krug, K., Ptito, M., D'Arceuil, H., Croxson, P. L., Johnson, P. J., Howells, H., Forkel, S. J., Dell'Acqua, F., & Catani, M. (2020). Differences in frontal network anatomy across primate species. *Journal of Neuroscience*, *40*(10), 2094–2107. https://doi.org/10.1523/JNEUROSCI.1650-18.2019

Beckmann, C. F. (2012). Modelling with independent components. *NeuroImage*, *62*(2), 891–901. https://doi.org/10.1016/j.neuroimage.2012.02.020

Beyh, A., Dell'Acqua, F., Cancemi, D., De Santiago Requejo, F., Ffytche, D., & Catani, M. (2022). The medial occipital longitudinal tract supports early stage encoding of visuospatial information. *Communications Biology*, *5*(1), 1. https://doi.org/10.1038/s42003-022-03265-4

Binkofski, F., Amunts, K., Stephan, K. M., Posse, S., Schormann, T., Freund, H.-J., Zilles, K., & Seitz, R. J. (2000). Broca's region subserves imagery of motion: A combined cytoarchitectonic and fmri study. *Human Brain Mapping*, *11*(4), 273–285. https://doi.org/10.1002/1097-0193(200012)11:4<273::AID-HBM40>3.0.CO;2-0

Casamitjana, A., Mancini, M., Robinson, E., Peter, L., Annunziata, R., Althonayan, J., Crampsie, S., Blackburn, E., Billot, B., Atzeni, A., et al. (2024). A next-generation, histological atlas of the human brain and its application to automated brain mri segmentation. *bioRxiv*, 2024.02.05.579016. https://doi.org/10.1101/2024.02.05.579016

Catani, M., Allin, M. P., Husain, M., Pugliese, L., Mesulam, M.-M., Murray, R. M., & Jones, D. K. (2007). Symmetries in human brain language pathways correlate with verbal recall. *Proceedings of the National Academy of Sciences*, *104*(43), 17163–17168. https://doi.org/10.1073/pnas.0702116104

Catani, M., & Bambini, V. (2014). A model for social communication and language evolution and development (scaled). *Current Opinion in Neurobiology*, *28*, 165–171. https://doi.org/10.1016/j.conb.2014.07.018

Catani, M., Dell'acqua, F., Vergani, F., Malik, F., Hodge, H., Roy, P., Valabregue, R., & Thiebaut de Schotten, M. (2012). Short frontal lobe connections of the human brain. *Cortex*, *48*(2), 273–291. https://doi.org/10.1016/j.cortex.2011.12.001

Catani, M., Jones, D. K., Donato, R., & Ffytche, D. H. (2003). Occipito-temporal connections in the human brain. *Brain*, *126*(9), 2093–2107. https://doi.org/10.1093/brain/awg203

Catani, M., Jones, D. K., & ffytche, D. H. (2005). Perisylvian language networks of the human brain. *Annals of Neurology*, *57*(1), 8–16. https://doi.org/10.1002/ana.20319

Catani, M., Mesulam, M.-M., Jakobsen, E., Malik, F., Martersteck, A., Wieneke, C., Thompson, C. K., Thiebaut de Schotten, M., Dell'Acqua, F., Weintraub, S., & Rogalski, E. (2013). A novel frontal pathway underlies verbal fluency in primary progressive aphasia. *Brain*, *136*(8), 2619–2628. https://doi.org/10.1093/brain/awt163

Catani, M., & Thiebaut de Schotten, M. (2008). A diffusion tensor imaging tractography atlas for virtual in vivo dissections. *Cortex*, *44*(8), 1105–1132. https://doi.org/10.1016/j.cortex.2008.05.004

Cattell, R. B. (1966). The scree test for the number of factors. *Multivariate Behavioral Research*, *1*(2), 245–276. https://doi.org/10.1207/s15327906mbr0102_10

Collins, A., & Koechlin, E. (2012). Reasoning, learning, and creativity: Frontal lobe function and human decision-making. *PLOS Biology*, *10*(3), e1001293. https://doi.org/10.1371/journal.pbio.1001293

Cousineau, M., Jodoin, P.-M., Garyfallidis, E., Côté, M.-A., Morency, F., Rozanski, V., Grand'Maison, M., Bedell, B., & Descoteaux, M. (2017). A test-retest study on parkinson's ppmi dataset

yields statistically significant white matter fascicles. *NeuroImage: Clinical*, *16*, 222–233. https://doi.org/10.1016/j.nicl.2017.07.020

Croxson, P. L., Forkel, S. J., Cerliani, L., & Thiebaut De Schotten, M. (2018). Structural variability across the primate brain: A cross-species comparison. *Cerebral Cortex*, *28*(11), 3829–3841. https://doi.org/10.1093/cercor/bhx244

de Benedictis, A., Efisio Marras, C., Petit, L., & Sarubbo, S. (2021). The inferior fronto-occipital fascicle: A century of controversies from anatomy theaters to operative neurosurgery [https://hal.science/hal-03345943]. *Journal of Neurosurgical Sciences*.

Dell'Acqua, F., & Catani, M. (2012). Structural human brain networks: Hot topics in diffusion tractography. *Current Opinion in Neurology*, *25*(4), 375–383. https://doi.org/10.1097/WCO.0b013e328355d544

Dell'Acqua, F., Lacerda, L., Barrett, R., D'Anna, L., Tsermentseli, S., Goldstein, L., & Catani, M. (2015). Megatrack: A fast and effective strategy for group comparison and supervised analysis of large-scale tractography datasets [https://archive.ismrm.org/2015/2843.html]. *Proc. Int. Soc. Magn. Reson. Med*, *23*, 2843.

Dell'Acqua, F., Lacerda, L., Catani, M., & Simmons, A. (2014). Anisotropic power maps: A diffusion contrast to reveal low anisotropy tissues from hardi data. *Proceedings Joint Annual Meeting ISMRM/ESMRMB*, 0730.

Dell'acqua, F., Scifo, P., Rizzo, G., Catani, M., Simmons, A., Scotti, G., & Fazio, F. (2010). A modified damped richardson-lucy algorithm to reduce isotropic background effects in spherical deconvolution. *NeuroImage*, *49*(2), 1446–1458. https://doi.org/10.1016/j.neuroimage.2009.09.033

Dell'Acqua, F., Simmons, A., Williams, S. C., & Catani, M. (2013). Can spherical deconvolution provide more information than fiber orientations? hindrance modulated orientational anisotropy, a true-tract specific index to characterize white matter diffusion. *Human Brain Mapping*, *34*(10), 2464–2483. https://doi.org/10.1002/hbm.22080

Dell'Acqua, F., & Tournier, J.-D. (2019). Modelling white matter with spherical deconvolution: How and why? *NMR in Biomedicine*, *32*(4), e3945. https://doi.org/10.1002/nbm.3945

Dick, A. S., & Tremblay, P. (2012). Beyond the arcuate fasciculus: Consensus and controversy in the connectional anatomy of language. *Brain*, *135*(12), 3529–3550. https://doi.org/10.1093/brain/aws222

Dickscheid, T., Gui, X., Simsek, A. N., Koehnen, L., Marcenko, V., Schiffer, C., Bludau, S., & Amunts, K. (2024). *Siibra-python (version v1.0a14)*. https://doi.org/10.5281/zenodo.7885728

Duffau, H., Moritz-Gasser, S., & Mandonnet, E. (2014). A re-examination of neural basis of language processing: Proposal of a dynamic hodotopical model from data provided by brain stimulation mapping during picture naming. *Brain and Language*, *131*, 1–10. https://doi.org/10.1016/j.bandl.2013.05.011

Dziedzic, T. A., Balasa, A., Jeżewski, M. P., Michałowski, Ł., & Marchel, A. (2021). White matter dissection with the klingler technique: A literature review. *Brain Structure & Function*, *226*(1), 13–47. https://doi.org/10.1007/s00429-020-02157-9

Fonov, V., Evans, A. C., Botteron, K., Almli, C. R., McKinstry, R. C., Collins, D. L., & Group, B. D. C. (2011). Unbiased average age-appropriate atlases for pediatric studies. *NeuroImage*, *54*(1), 313–327. https://doi.org/10.1016/j.neuroimage.2010.07.033

Forkel, S., Bortolami, C., Dulyan, L., Barrett, R. L., & Beyh, A. (2024). Dissecting white matter pathways: A neuroanatomical approach. https://doi.org/10.31234/osf.io/9xwgm

Forkel, S. J., & Catani, M. (2019). Diffusion imaging methods in language sciences. In G. I. de Zubicaray & N. O. Schiller (Eds.), *The oxford handbook of neurolinguistics*. Oxford University Press. https://doi.org/10.1093/oxfordhb/9780190672027.013.9

Forkel, S. J., Thiebaut de Schotten, M., Dell'Acqua, F., Kalra, L., Murphy, D. G., Williams, S. C., & Catani, M. (2014). Anatomical predictors of aphasia recovery: A tractography study of bilateral perisylvian language networks. *Brain*, *137*(7), 2027–2039. https://doi.org/10.1093/brain/awu113

Forkel, S. J., Thiebaut de Schotten, M., Kawadler, J. M., Dell'Acqua, F., Danek, A., & Catani, M. (2014). The anatomy of fronto-occipital connections from early blunt dissections to contemporary tractography. *Cortex*, *56*, 73–84. https://doi.org/10.1016/j.cortex.2012.09.005

Giampiccolo, D., & Duffau, H. (2022). Controversy over the temporal cortical terminations of the left arcuate fasciculus: A reappraisal. *Brain*, *145*(4), 1242–1256. https://doi.org/10.1093/brain/awac057

Hagoort, P. (2013). Muc (memory, unification, control) and beyond. *Frontiers in Psychology*, *4*, 416. https://doi.org/10.3389/fpsyg.2013.00416

Hagoort, P. (2019). The neurobiology of language beyond single-word processing. *Science*, *366*(6461), 55–58. https://doi.org/10.1126/science.aax0289

Hickok, G., & Poeppel, D. (2004). Dorsal and ventral streams: A framework for understanding aspects of the functional anatomy of language. *Cognition*, *92*(1–2), 67–99. https://doi.org/10.1016/j.cognition.2003.10.011

Hickok, G., & Poeppel, D. (2007). The cortical organization of speech processing. *Nature Reviews Neuroscience*, *8*(5), 393–402. https://doi.org/10.1038/nrn2113

Hintz, F., Dijkhuis, M., van 't Hoff, V., McQueen, J. M., & Meyer, A. S. (2020). A behavioural dataset for studying individual differences in language skills. *Scientific Data*, *7*(1), 429. https://doi.org/10.1038/s41597-020-00758-x

Jeurissen, B., Leemans, A., Tournier, J.-D., Jones, D. K., & Sijbers, J. (2013). Investigating the prevalence of complex fiber configurations in white matter tissue with diffusion magnetic resonance imaging. *Human Brain Mapping*, *34*(11), 2747–2766. https://doi.org/10.1002/hbm.22099

Jolliffe, I. T., & Cadima, J. (2016). Principal component analysis: A review and recent developments. *Philosophical Transactions of the Royal Society A: Mathematical, Physical and Engineering Sciences*, *374*(2065), 20150202. https://doi.org/10.1098/rsta.2015.0202

Jones, D. K. (2003). Determining and visualizing uncertainty in estimates of fiber orientation from diffusion tensor mri. *Magnetic Resonance in Medicine*, *49*(1), 7–12. https://doi.org/10.1002/mrm.10331

Kellner, E., Dhital, B., Kiselev, V. G., & Reisert, M. (2016). Gibbs-ringing artifact removal based on local subvoxel-shifts. *Magnetic Resonance in Medicine*, *76*(5), 1574–1581. https://doi.org/10.1002/mrm.26054

Liakos, F., Komaitis, S., Drosos, E., Neromyliotis, E., Skandalakis, G. P., Gerogiannis, A. I., Kalyvas, A. V., Troupis, T., Stranjalis, G., & Koutsarnakis, C. (2021). The topography of the frontal terminations of the uncinate fasciculus revisited through focused fiber dissections: Shedding light on a current controversy and introducing the insular apex as a key anatomoclinical area. *World Neurosurgery*, *152*, e625–e634. https://doi.org/10.1016/j.wneu.2021.06.012

McInnes, L., Healy, J., & Melville, J. (2020). Umap: Uniform manifold approximation and projection for dimension reduction. *arXiv preprint arXiv:1802.03426*. https://doi.org/10.48550/arXiv.1802.03426

Nozais, V., Forkel, S. J., Foulon, C., Petit, L., & Thiebaut de Schotten, M. (2021). Functionnectome as a framework to analyse the contribution of brain circuits to fmri. *Communications Biology*, *4*(1), 1–12. https://doi.org/10.1038/s42003-021-02530-2

Nozais, V., Theaud, G., Descoteaux, M., Thiebaut de Schotten, M., & Petit, L. (2023). Improved functionnectome by dissociating the contributions of white matter fiber classes to functional activation. *Brain Structure and Function*, *228*(9), 2165–2177. https://doi.org/10.1007/s00429-023-02714-y

Ocklenburg, S., Friedrich, P., Güntürkün, O., & Genç, E. (2016). Intrahemispheric white matter asymmetries: The missing link between brain structure and functional lateralization? *Reviews in the Neurosciences*, *27*(5), 465–480. https://doi.org/10.1515/revneuro-2015-0052

Oishi, K., Zilles, K., Amunts, K., Faria, A., Jiang, H., Li, X., Akhter, K., Hua, K., Woods, R., Toga, A. W., et al. (2008). Human brain white matter atlas: Identification and assignment of common anatomical structures in superficial white matter. *NeuroImage*, *43*(3), 447–457. https://doi.org/10.1016/j.neuroimage.2008.07.009

Rojkova, K., Volle, E., Urbanski, M., Humbert, F., Dell'Acqua, F., & Thiebaut de Schotten, M. (2016). Atlasing the frontal lobe connections and their variability due to age and education: A spherical deconvolution tractography study. *Brain Structure and Function*, *221*(3), 1751–1766. https://doi.org/10.1007/s00429-015-1001-3

Saur, D., Lange, R., Baumgaertner, A., Schraknepper, V., Willmes, K., Rijntjes, M., & Weiller, C. (2006). Dynamics of language reorganization after stroke. *Brain*, *129*(6), 1371–1384. https://doi.org/10.1093/brain/awl090

Schilling, K. G., Gao, Y., Janve, V., Stepniewska, I., Landman, B. A., & Anderson, A. W. (2018). Confirmation of a gyral bias in diffusion mri fiber tractography. *Human Brain Mapping*, *39*(3), 1449–1466. https://doi.org/10.1002/hbm.23936

Schilling, K. G., Rheault, F., Petit, L., Hansen, C. B., Nath, V., Yeh, F.-C., Girard, G., Barakovic, M., Rafael-Patino, J., Yu, T., et al. (2021). Tractography dissection variability: What happens when 42 groups dissect 14 white matter bundles on the same dataset? *NeuroImage*, *243*, 118502. https://doi.org/10.1016/j.neuroimage.2021.118502

Shekari, E., & Nozari, N. (2023). A narrative review of the anatomy and function of the white matter tracts in language production and comprehension. *Frontiers in Human Neuroscience*, *17*. https://doi.org/10.3389/fnhum.2023.1139292

Sherwood, C. C., & Smaers, J. B. (2013). What's the fuss over human frontal lobe evolution? *Trends in Cognitive Sciences*, *17*(9), 432–433. https://doi.org/10.1016/j.tics.2013.06.008

Smaers, J. B., Schleicher, A., Zilles, K., & Vinicius, L. (2010). Frontal white matter volume is associated with brain enlargement and higher structural connectivity in anthropoid primates. *PLOS ONE*, *5*(2), e9123. https://doi.org/10.1371/journal.pone.0009123

Smaers, J. B., Steele, J., Case, C. R., Cowper, A., Amunts, K., & Zilles, K. (2011). Primate prefrontal cortex evolution: Human brains are the extreme of a lateralized ape trend. *Brain Behavior and Evolution*, *77*(2), 67–78. https://doi.org/10.1159/000323671

Talozzi, L., Forkel, S. J., Pacella, V., Nozais, V., Allart, E., Piscicelli, C., Pérennou, D., Tranel, D., Boes, A., Corbetta, M., et al. (2023). Latent disconnectome prediction of long-term cognitive-behavioural symptoms in stroke. *Brain*, *146*(5), 1963–1978. https://doi.org/10.1093/brain/awad013

Thiebaut de Schotten, M., Dell'Acqua, F., Valabregue, R., & Catani, M. (2012). Monkey to human comparative anatomy of the frontal lobe association tracts. *Cortex*, *48*(1), 82–96. https://doi.org/10.1016/j.cortex.2011.10.001

Thiebaut de Schotten, M., ffytche, D. H., Bizzi, A., Dell'Acqua, F., Allin, M., Walshe, M., Murray, R., Williams, S. C., Murphy, D. G., & Catani, M. (2011). Atlasing location, asymmetry and inter-subject variability of white matter tracts in the human brain with mr diffusion tractography. *NeuroImage*, *54*(1), 49–59. https://doi.org/10.1016/j.neuroimage.2010.07.055

Türe, U., Yaşargil, M. G., Friedman, A. H., & Al-Mefty, O. (2000). Fiber dissection technique: Lateral aspect of the brain. *Neurosurgery*, *47*(2), 417–426. https://doi.org/10.1097/00006123-200008000-00028

Ueno, T., Saito, S., Rogers, T. T., & Lambon Ralph, M. A. (2011). Lichtheim 2: Synthesizing aphasia and the neural basis of language in a neurocomputational model of the dual dorsal-ventral language pathways. *Neuron*, *72*(2), 385–396. https://doi.org/10.1016/j.neuron.2011.09.013

Varriano, F., Pascual-Diaz, S., & Prats-Galino, A. (2020). Distinct components in the right extended frontal aslant tract mediate language and working memory performance: A tractography-

informed vbm study. *Frontiers in Neuroanatomy*, *14*. https://doi.org/10.3389/fnana.2020.00021

Vassal, F., Schneider, F., Boutet, C., Jean, B., Sontheimer, A., & Lemaire, J.-J. (2026). Combined dti tractography and functional mri study of the language connectome in healthy volunteers: Extensive mapping of white matter fascicles and cortical activations. *PLOS ONE*, *11*(3), e0152614. https://doi.org/10.1371/journal.pone.0152614

Vavassori, L., Sarubbo, S., & Petit, L. (2021). Hodology of the superior longitudinal system of the human brain: A historical perspective, the current controversies, and a proposal. *Brain Structure and Function*, *226*(5), 1363–1384. https://doi.org/10.1007/s00429-021-02265-0

Veraart, J., Fieremans, E., & Novikov, D. S. (2016). Diffusion mri noise mapping using random matrix theory. *Magnetic Resonance in Medicine*, *76*(5), 1582–1593. https://doi.org/10.1002/mrm.26059

Weiller, C., Reisert, M., Peto, I., Hennig, J., Makris, N., Petrides, M., Rijntjes, M., & Egger, K. (2021). The ventral pathway of the human brain: A continuous association tract system. *NeuroImage*, *234*, 117977. https://doi.org/10.1016/j.neuroimage.2021.117977

Winkler, A. M., Ridgway, G. R., Webster, M. A., Smith, S. M., & Nichols, T. E. (2014). Permutation inference for the general linear model. *NeuroImage*, *92*, 381–397. https://doi.org/10.1016/j.neuroimage.2014.01.060

Yendiki, A., Aggarwal, M., Axer, M., Howard, A. F. D., van Walsum, A.-M. v. C., & Haber, S. N. (2022). Post mortem mapping of connectional anatomy for the validation of diffusion mri. *NeuroImage*, *256*, 119146. https://doi.org/10.1016/j.neuroimage.2022.119146

Zhang, F., Daducci, A., He, Y., Schiavi, S., Seguin, C., Smith, R. E., Yeh, C.-H., Zhao, T., & O'Donnell, L. J. (2022). Quantitative mapping of the brain's structural connectivity using diffusion mri tractography: A review. *NeuroImage*, *249*, 118870. https://doi.org/10.1016/j.neuroimage.2021.118870